MJO-induced Warm Pool Eastward Extension in Connection to the Onset of El Niño: Observations from 1998-2019

Yakelyn R. Jauregui,[1] Shuyi S. Chen,[1]

[1] *Department of Atmospheric Sciences, University of Washington, Seattle, Washington*

Submitted to *Journal of Climate*

Corresponding author: Yakelyn R. Jauregui, yakelynr@uw.edu

ABSTRACT

The Madden-Julian Oscillation (MJO) and El Niño Southern Oscillation (ENSO) are the two most important tropical phenomena that affect global weather and climate on intraseasonal and interannual timescales. Although they occur on different timescales, the MJO-induced sea-surface temperature (SST) anomalies over the western Pacific have spatial scales similar to SST anomalies prior to the onset of El Niño. This study aims to address the question of whether the MJO plays an important role in the warm pool eastward extension (WPEE) leading up to the onset of El Niño. We use over 20 years of satellite observations, including optimum interpolated SST, TRMM-GPM precipitation, and the cross calibrated multi-platform (CCMP) surface winds from 1998-2019 to quantify the spatial structure and duration of the MJO-induced warm SST anomalies over the equatorial Pacific (120°E-170°E, 10°S–10°N). The intensity of the MJO is measured by the total rain volume and average surface westerly windspeed throughout its lifetime. Results show that 1) 65% of the MJO events induced a WPEE up to 3000 km along the equator, which can last beyond 15 days; 2) the MJO events that precede the onset of El Niño are generally stronger and produce significant WPEE far beyond its annual cycle (~1000 km); 3) consecutive MJO events can produce much larger WPEE prior to El Niño, which are observed in all El Niño events from 1998-2019; and 4) more frequent and larger MJO-induced WPEE occur in March-May than other seasons. These results help understand the MJO-ENSO interaction and improve the prediction of the onset of El Niño.

1. Introduction

El Niño Southern-Oscillation (ENSO) is the dominant mode of interannual (2-7 years) variability that modulates the global weather and climate (Philander et al. 1984). ENSO consists of alternating periods of anomalously warm and cold ocean conditions in the Pacific, with considerable irregularity in amplitude, duration, temporal evolution, and spatial structure of these events (Wyrtki 1975; Cane 1986; Jin 1997; Neelin et al. 1998; Fedorov and Philander 2001; Wang et al. 2012). On the intraseasonal timescale (30-90 days), the Madden-Julian Oscillation (MJO) (Madden and Julian 1971, 1972) typically initiates over the equatorial Indian Ocean as large-scale precipitation with anomalous zonal winds and propagate eastward to the west Pacific. The MJO affects the atmosphere and ocean across different spatial and temporal scales (e.g., Zhang 2013) and acts as a primary source of sub-seasonal predictability of global weather (Rui and Wang 1990; Yano et al. 2004; Zhang 2005, 2013). The MJO and ENSO account for most of the tropical climate variability. Although they occur at widely separated timescales, they can interact, especially over the West Pacific warm pool (Kessler and Kleeman 2000; Bergman et al. 2001; Lengaigne et al. 2002).

Observational evidence suggests that El Niño may require an initial surface and subsurface warming across the Pacific (Kessler 2002). This initial warming is named the onset of El Niño in the central Pacific. It is observed as a warm pool eastward extension (WPEE) far beyond its climatological position. The MJO contribution to the onset of El Niño has been suggested based on its plausible mechanisms to warm the central and eastern Pacific in observations (Lau and Chan 1988; Kessler et al. 1995; Anderson et al. 1996; Bergman et al. 2001; Zhang and Gottschalck 2002; Maes et al. 2002, 2006; Bosc et al. 2009), and modeling studies (McPhaden and Yu 1999; Kessler and Kleeman 2000; Susuki and Takeuchi 2000; Lengaigne et al. 2002, 2003).

There are two main physical mechanisms identified by previous studies through which the MJO can induce a WPEE. First, Kessler et al., (1995) pointed out the role of the MJO westerly wind bursts (WWB) forcing an eastward propagating downwelling equatorial wave that deepens the thermocline and induces eastward surface current anomalies enabling the advection of warm waters to the east. This substantial oceanic dynamical response to MJO-westerlies is enhanced if consecutive MJO events occur, resulting in a weaker horizontal temperature gradient. Second, Anderson et al. (1996), based on observations from TOGA-COARE, highlighted the importance of the MJO-induced upper ocean stratification that occurs. The vigorous WWB increases the mixed layer (ML) depth. At the same time, the MJO-rainfall reduces the ocean surface layer's density, resulting in an upper ocean's stratification. A shallower ML forms within a deeper isothermal layer called barrier layer, particularly in the far western Pacific, where rainfall dominates evaporation (BL, Lukas and Lindstrom 1991). Over time, after the passage of the MJO, in calm wind and clear sky conditions, the BL serves as an essential blockade that prevents the cold thermocline water from entering the ML. The shallower ML and the presence of a thick enough BL allow maximum upper-ocean warming by retaining a significant portion of the shortwave radiation, which strengthen the initial stratification (Anderson et al., 1996, Vialard and Delecluse 1998; Maes et al. 2002, 2006).

The two air-sea interactive processes associated with the MJO, namely the dynamics of WWB-oceanic Kelvin wave identified by Kessler et al. (1995) and the upper ocean stratification of rainfall- development of BL maintaining warm SST as observed by Anderson et al. (1996), are key to understand this MJO-ENSO interaction. Together they act to reduce the east-west temperature gradient, which allows a further shift of the warm pool eastward during the onset of El Niño (McPhaden and Picaut 1990; Delcroix et al. 1994; Kessler and

92 Kleeman 2000; Susuki and Takeuchi 2000; Lengaigne et al. 2003). The MJO impact on the
93 upper ocean dynamics and thermodynamics favors the WPEE and maintenance of warm
94 SSTs that could last from several days to weeks after the passage of the MJO. These previous
95 studies have suggested that these shorter timescale impacts of the MJO-induced WPEE
96 control the SST in the central Pacific, a key region for atmospheric-ocean coupled
97 interactions, where the presence of a shallower ML and the existence of a BL can enhance the
98 momentum forcing advecting warmer waters further east.

99 The well-known sea-surface warming in the central and eastern Pacific induced by
100 oceanic Kelvin waves has been widely studied in the context of El Niño initiation or
101 amplification. However, in the western Pacific, WWBs are often associated with tropical
102 convection, which are often observed prior and/or during the 1982-83, 1991-92, 1997-98 El
103 Niño events (Harrison 1984; Lau and Chan 1988; Kessler et al., 1995; Mcphaden 1999;
104 Bergman et al., 2001). Vecchi and Harrison (2000) showed that equatorial WWBs can
105 substantially alter the SST (up to 1C) over the entire Pacific after 80 days; however, they did
106 not distinguish WWBs based on tropical phenomena that caused them (i.e., tropical cyclones
107 versus MJO events). Then, Chiodi et al., (2014) showed that MJO with embedded WWBs can
108 induce warming (up to 0.6C) in the eastern Pacific from 20-80 days; but MJO without WWBs
109 does not affect the SST change. Other studies (Seiki and Takayabu 2007, Puy et al., 2016)
110 have demonstrated that nearly all strong WWB occurred in the convective MJO phase.
111 Furthermore, the sustained MJO-westerlies are much more effective in generating a large-
112 scale coherent sea-surface warming (Fasullo and Webster 2000). Thus, in contrast to previous
113 studies, this paper is interested on the characterization (e.g., duration, extent) of MJO-induced
114 sea-surface warming that occurs immediately after the passage of the MJO event. We do so
115 by looking at the post-MJO WPEE.

116 The warm pool SST exceeds the threshold for deep atmospheric convection (e.g., Graham
117 and Barnett 1987), and when the warm pool extends to the central Pacific, deep convection
118 can occur, providing with mid-tropospheric heat source driving a large-scale atmosphere-
119 ocean coupled interaction and triggering El Niño event. Knowing how much and for how
120 long one or multiple MJO events induce a WPEE is essential, particularly to the El Niño
121 prediction. Larger WPEE weakens the large-scale east-west SST gradient which allows for
122 further WPEE spinning up positive atmosphere-ocean coupling that characterizes the El Niño
123 initiation and development (Kessler et al., 1995; Bergman et a., 2001; Kessler and Kleeman
124 2000).

125 The MJO can contribute to the onset of El Niño; however, the evolution of El Niño from
126 an early stage to a fully developed phase depends on favorably ocean dynamics, in
127 conjunction with air-sea interactions to strengthen and prolong the SST warming (Harrison
128 and Schopf 1984; Wyrtki 1985; McPhaden and Yu 1999; Bergman et al. 2001; Kessler 2002;
129 Battisti et al. 2019). Despite the efforts to investigate the MJO-ENSO interaction as
130 summarized in Zhang et al. (2001) and many modeling and observational studies mentioned
131 above, the contribution by the MJO to WPEE and its relation to ENSO has never been
132 quantified in time and space with a significant number of the MJO events using long-term
133 observations.

134 In this study, nearly 100 MJO events identified using more than 20 years of
135 unprecedented multi-satellite precipitation data (Kerns and Chen 2020) along with surface
136 wind and SST observations are used to provide quantitative analyses of the MJO-induced
137 WPEE over the western Pacific. We quantify both the spatial structure and duration of the
138 MJO-induced WPEE for individual and consecutive MJO events in relation to the onset of
139 the six El Niño events that occurred from 1998–2019. The examination of subsurface ocean

thermodynamic and dynamic change associated with the WPEE is beyond the scope of this study due to the lack of reliable ocean data at higher spatial and temporal resolution.

The remainder of this paper is organized as the following: Section 2 describes the observational data sets and the methods used in this study to quantify the duration and intensity of each MJO event, and the MJO-induced WPEE. Section 3 demonstrates how we analyze the spatial structure and duration of the MJO-induced WPEE and their relationship to the onset of El Niño using two specific examples. Section 4 provides comprehensive analyses of all the MJO and ENSO events observed during 1998-2019, including statistics of MJO-induced WPEE in time and space as well as a composite of warming due to the MJO over the west-central Pacific. Section 5 further demonstrates that the WPEE is a robust signal above seasonal variability by removing the annual cycle. Section 6 examines the warm pool displacement in relation to the intensity of the MJO as defined by its total precipitation and strength of surface westerly winds. Summary and conclusions are given in Section 7.

2. Data and Methods

a. Precipitation, wind, and SST Data

The Tropical Rainfall Measuring Mission (TRMM) Multi-satellite Precipitation Analysis (TMPA) 3B43 V7 data from June 1998-June 2019 is used to identify the MJO event (Kerns and Chen 2016, 2020). TMPA estimates instantaneous rain rates at 3-hourly on a regular 0.25° grid based on passive-microwave and infrared retrievals (Huffman et al. 2007).

The Cross-Calibrated Multi-Platform version 2 (CCMP V2) wind at 10 m is used to characterize the surface wind associated with the MJO events from June 1998-June 2019. The 6-hourly and 0.25^{o} resolution CCMP V2 wind product is produced by Remote Sensing

Systems (REMSS) (Atlas et al. 2008). It combines surface wind data from satellite radiometer retrievals, QuikSCAT and ASCAT satellite scatterometer measurements, moored buoys, and ERA-Interim reanalysis using a variational analysis method.

The daily SST data used in this study is from the National Ocean Atmospheric Administration (NOAA) Optimum Interpolation Sea Surface Temperature version 2 (OISST-V2, Reynolds et al. 2002, 2007) at 0.25° spatial resolution. The Niño 3.4 (5°S-5°N, 170°E-120°W) SST monthly anomalies are obtained from the NOAA Climate Prediction Center (CPC) for real-time ENSO monitoring indexes (https://www.cpc.ncep.noaa.gov/data/indices/sstoi.indices). These data coverage is from June 1998–June 2019.

b. MJO identification

The MJO events are identified based on the large-scale precipitation tracking (LPT) algorithm developed by Kerns and Chen (2016, 2020) using TMPA data. This method identifies the evolution of individual MJO events, or as LPT systems explicitly in time and space. A large-scale precipitation object (LPO) is first identified by 12 mm day^{-1} threshold contour using a 5^{o}x5^{o} spatial filter on 3-day accumulation of precipitation. The LPO is then tracked in time at 3-hourly interval as an LPT system. The MJO LPT is defined as an LPT system that last beyond 10 days with eastward propagation speed > 0 m s^{-1} as described in Kerns and Chen (2020). It provides the size, center locations, both zonal and meridional structure, and intensity (as described in 3.c) of the MJO events, which are not represented by other MJO indices such as the RMM (Wheeler and Hendon 2004). It is uniquely suited for studying the MJO impacts and air-sea interaction. Kerns and Chen (2020) provide a detailed

184 description and statistics of MJO events from 1998-2018. The MJO LPT events database is
185 extended to include 2019 in this study using the same methodology.

186 Two examples of the MJO LPT systems occurred in January-March 2002 and January-
187 February 2018 are shown in Figs. 1a and 1b, respectively (MJO-10 and MJO-93 in Fig. 10).
188 The 2002 MJO LPT system lasted about 50 days and propagated from the Indian Ocean to
189 the western Pacific with an average eastward speed of 1.7 m s^{-1}, while the 2018 MJO system
190 lasted for 36 days at 3.1 m s^{-1}. From hereafter, we refer to an MJO LPT system as an MJO
191 event.

192 The following analysis uses the following parameters from each MJO event obtained by
193 the algorithm: (1) the centroids associated with each LPO provides with time and location;
194 (2) the LPO provides the area of impact and allows the quantification of rainfall at a given
195 time. Each MJO event has an initial and ending time as illustrated in colors in Fig. 1.

196 To investigate the MJO-induced WPEE in relation to the onset of the El Niño, 98 MJO
197 events, a subset of more than 200 from June 1998 - June 2019, are selected as the MJO events
198 over the tropical western-central Pacific (130-180^{o}E) with LPT center latitude located
199 between 10^{o}S-10^{o}N and lasted beyond 10 days. This criterion ensures that MJO events
200 propagate over the Maritime Continent and stay in the equatorial western Pacific, beyond the
201 synoptic timescale. Other MJO identification methods do not allow subset MJO events with
202 direct impact on the equatorial warm pool.

203 *c. MJO intensity measured by precipitation and wind*

204 The MJO, by definition, is characterized as large-scale convection and circulation that
205 vary on the intraseasonal time scale with convectively active and suppressed phases as they
206 propagate eastward (Madden and Julian 1994; Zhang 2005). The convectively active

(suppressed) phase is associated with strong surface westerly (easterly) winds (Zhang 2005). The surface westerlies are usually stronger than the easterlies, which are enhanced by downward momentum transport within mesoscale convective systems (MCSs) in the convective active phase (Houze et al. 2000; Mechem et al. 2005). The convection and precipitation within the MJO large-scale envelope are dominated by MCSs (sometime referred to as cloud clusters) and have been observed to have multiscale variability from the diurnal, bi-diurnal, to synoptic timescales (e.g., Chen et al. 1996; Chen and Houze 1997a). The convection and surface wind vary among the MJO events and they are modulated directly by ENSO on interannual timescale over the warm pool (e.g., Chen and Houze 1997b). It is advantageous to characterize the strength of the MJO according to its total precipitation and surface westerly wind, which are two most important measures of the MJO impacts on the atmospheric circulation through latent heating and the upper ocean through input of freshwater and momentum.

Here we define the intensity of the MJO as 1) an accumulated total rain volume from inside of each LPO through the entire MJO LPTs (in m^3), and 2) 6-hourly maximum surface westerly winds (in m s^{-1}) inside each LPO and are averaged throughout the lifetime of each MJO LPTs (Fig. 2). The MJO envelope indicates the area encompassed by the MJO LPTs feature smoothed with a 2.5° latitude/longitude Gaussian (purple contour in Fig. 2). The region 120°E–170°E and 10°S–10°N represents the area of MJO impact on the warm pool shown in a red box. The MJO intensity of convection over the warm pool is defined as the rain integrated over the overlapping region between the MJO envelope and the red box. Similarly, the intensity of WWB is the average of the maximum westerly winds over the same region in m s^{-1}. Thus, each MJO intensity is quantified in terms of rain volume (m^3) and WWB (m s^{-1}). The analysis is repeated by varying the selected areas to ensure that the results

231 are representative of the warm pool, e.g., 120°E–170°E, 120°E–180°, 130°E–180°,
232 130°E–170° in combination with 10°S–10°N, 15°S–15°N. The results (not shown) are
233 essentially the same.

234 *c. MJO-induced warm pool eastward extension (WPEE)*

235 The warm pool has traditionally been defined by various isotherms of the ocean surface
236 such as 28°C, 28.5°C, or 29°C in previous studies (Picaut and Delcroix 1995; Clarke et al.
237 2000; McPhaden and Picaut 1990; Picaut et al. 2001). This study defines the warm pool as
238 the 28.5°C isotherm because it is generally representative of the large-scale warm pool
239 feature over the tropical Pacific. The warm pool evolution and the extent of eastward
240 displacement estimation use absolute values of SST because it is more critical than anomalies
241 in activating convection (Graham and Barnett 1987; Jauregui and Takahashi 2018). The high-
242 frequency SST variability was excluded using a 3-day centered SST moving mean and a two-
243 dimensional Gaussian smoother with a standard deviation of 10 grid points (2.5°,
244 approximately 250 km near the equator).

245 To examine whether the warm pool displacement is primarily associated with MJO events
246 or resulting from the annual cycle, we computed the warm pool anomaly as follows. First, the
247 warm pool daily climatology is the 28.5°C isotherm obtained from the daily SST climatology
248 that only retains the first three harmonics of the annual cycle from 1982 – 2010. To illustrate
249 the spatial variability of the warm pool we show the monthly climatology in Fig. 3. Second,
250 the warm pool anomaly is computed by removing the daily warm pool easternmost longitude
251 from its daily climatology, from 10°S to 10°N (Fig. 4b, d). For instance, the warm pool
252 anomaly on April 12, 2002 is about 3,000 km close to the equator, and more significant
253 anomalies are observed off and north of the equator. In contrast, shorter warm pool anomaly

254 is observed on March 8, 2018 in the north and about -3,000 km south of the equator. The
255 warm pool climatology (Fig. 3) has a strong spatial variability particularly off the equator,
256 associated with the seasonal sun migration. It extends eastward in the north while it retreats in
257 the south. Section 5a describes the seasonal warm pool migration in relation to the MJO
258 propagation in the western Pacific.

259 The warm pool eastern longitude extends eastward after the passage of the MJO event (s)
260 (Fig. 10a, b). Thus, given the physical mechanisms that explain the post-MJO WPEE above,
261 we track the anomalous warm pool eastern edge immediately after the passage of MJO. To do
262 so, Day-0 refers to the MJO ending date and Day-1 to the following day. Then, the warm
263 pool eastern edge anomaly structure is tracked for each day from Day-0 until it reaches a
264 maximum eastward displacement that occurs at Day-max, defined in the next section. Figure
265 4 shows the warm pool anomaly at Day-max after the MJO events illustrated in Fig. 1, and
266 Fig. 5 illustrate the absolute warm pool evolution from Day-0 to Day-max.

267 This method is different from Drushka et al. (2015) that studied the mechanisms of the
268 intraseasonal equatorial (2°S-2°N) warm pool eastern edge (28.5°C) displacement 10-days
269 following with WWBs and during the active MJO phase using RMM index 6-7 phase. Our
270 method focuses on the WPEE after the MJO passage over the equatorial western Pacific
271 without assuming any timing constraint (e.g., 10 days).

272 *d. WPEE quantification*

273 The WPEE is quantified as the warm pool easternmost longitude difference at each
274 day post-MJO, relative to the longitude at Day-0, from 10°S to 10°N, every 0.25° (Fig. 6 a,
275 d). To remove the seasonal variability of the warm pool, we also quantified the WPEE
276 anomalous displacement using anomalies quantified in Section 2c and showed in Fig. 4b, d.

To identify the maximum post-MJO WPEE and Day-max, we use the equatorial band (5°S - 5°N) averaged absolute and anomalous displacement (Fig. 6c, f). A 5-day centered mean is applied to remove high-frequency variability and allow continuous tracking of the large-scale warm pool displacement. The smoothed equatorial band of the warm pool displacement is tracked in time until it reaches the maximum WPEE that occurs at Day-max, allowing short (< 500 km) and temporary (< 7 days) retreat as shown in Fig. 6c, f.

This method allows us to quantify the temporal and spatial WPEE after MJO events. For instance, the post-MJO WPEE associated with the MJO event illustrated in Fig. 1a (MJO-11 in Fig. 10) is about 2500 km from which 2000 km is an anomalous displacement (Fig. 6c) and occurred on April 12, 2002, after 37 days of the MJO event. In contrast, the post-MJO WPEE in Fig. 5f is less than 500 km and occurred on March 8, 2018, 18 days after the MJO event showed in Fig. 1b (MJO-93 in Fig. 10).

65 out of 98 MJO events were associated with a post-MJO WPEE, and the warm pool retreated or did not move for the remaining events. To compare MJO events with and without influence on the WPEE, we use the same method and criteria to compute the maximum westward displacement when the post-MJO WPEE does not occur.

Our main results are not sensitive to the use of absolute or anomalous WPEE because we use the equatorial band to find the maximum WPEE and Day-max; however, we use the anomalous WPEE to avoid the influence of the seasonal cycle. Our results are based on the parameters related to the MJO and post-MJO warm pool displacement parameters (e.g., WPEE duration, MJO duration in the western Pacific) shown in Appendix Figure A1.

3. Spatial structure and duration of MJO-induced WPEE and the El Niño onset

300 Tracking the MJO events using the LPT algorithm, as described in Section 2.b., made it
301 possible to investigate the spatial and temporal structure and evolution of the MJO-induced
302 SST changes during and post-MJO event in this study for the first time. This section
303 exemplifies the importance of consecutive high frequency but large-scale MJO forcing, often
304 observed prior to El Niño development (Kessler et al., 1995; McPhaden, 1999; Boulanger and
305 Menkes, 1999; Bergman et al., 2001), as observed in 2002 and 2018.

306 The La Niña conditions in 2001 transitioned to El Niño onset in 2002 associated with the
307 WPEE that occurred only after the intense and consecutive WWBs associated with MJO
308 events observed from October 2001 to early March 2002 (McPhaden 2004, Fig. 7, MJO-7 to
309 MJO-10). Warmer waters reached Niño 3.4 region, leaving a much weaker large-scale zonal
310 SST gradient in April and May (Fig. 7d) that favored further convection and WWBs (MJO-
311 11) and the El Niño development conditions in June 2002. Similarly, a series of MJO events
312 from January to April 2018 (MJO-92 to MJO-95), during La Niña conditions (NOAA/CPC,
313 2017), preceded the WPEE leading up to the large-scale zonal SST gradient weakening in
314 April-May 2018 that favored El Niño onset in August in the same year (Fig. 8).

315 **The MJO-induced WPEE induces a large-scale and coherent SST anomaly as**
316 **illustrated in Fig. 9, from January to December 2002.** The spatial scale of SST anomalies
317 resemble the spatial scale of the anomalies observed at the onset and developing phase of El
318 Niño 2002 (Fig. 9d, e) and El Niño 2018 (not shown). However, the MJO-induced warming
319 occurs multiple times, each with much shorter time scales (e.g., weeks) and progressively
320 eastward with time. The large-scale warm anomalies associated with these MJO events
321 weaken the trade winds (Fig. 9c), which favors conditions for developing El Niño over the
322 central-eastern Pacific. In contrast, El Niño development and growth substantially affect the

SST and trade winds over the entire equatorial Pacific for months (Fig. 9 d,e). Motivated by the post-MJO WPEE observed before the onset of El Niño 2002 and 2018, we aim to address the following questions: (i) is the post-MJO WPEE a common feature? (ii) do consecutive MJO activity often occurs prior to the onset of El Niño? (iii) what are the magnitude and structure of the MJO-induced WPEE, and how do they relate to the MJO intensity of convection and westerlies?

4. The MJO and ENSO from 1998-2019

The relationship of the MJO, post-MJO WPEE, and El Niño onset is investigated using observations from 1998-2019. Figure 10 shows the observed eastern edge of the warm pool, its climatology, the MJO events, the warm pool anomaly, absolute zonal surface windspeed, and the Nino3.4 index representing ENSO conditions over the 21-year period. Tracking the post-MJO WPEE, as described in Section 2c and quantified in Section 2d, allow us to better understand the connection between the MJO activity and the onset of El Niño events from 1998-2019.

There were six El Niño and five La Niña events from 1998-2019 as shown by the Niño 3.4 index (Fig. 10). The NOAA declares the El Niño advisory when Niño 3.4 exceeds 0.5°C five consecutive overlapping three-month seasons. The onset of each El Niño event in this study corresponds to the first three-month season. These onset months are centered on June 2002, August 2004, September 2006, July 2009, October 2014, and October 2018 (red arrows in Fig. 10d). To examine the MJO events that could potentially contribute to the onset of El Niño, we located MJO events that occurred within 9 months before the onset. This period is chosen based on the robust 9-month lag correlation between precursors for the onset of El Niño (e.g., equatorial sea level, zonal mean thermocline) and the Niño 3.4 index showed by Kug et al. (2010). Using these criteria, we have identified 23 MJO events that occurred

before the onset of El Niño events (highlighted in red in Fig. 10a) and 33 MJO events during El Niño events (highlighted in dark red).

Enhanced MJO activity is followed by an anomalous WPEE (Fig. 10b) before each El Niño onset from 1998- 2019. We have identified 65 MJO-induced WPEE events, and 42 out of 65 of these events occurred not associated with El Niño event development (Table 1). 17 events occurred before the onset of El Niño events, 25 during El Niño events, and the remaining during neutral or La Niña conditions (Appendix Figure A1 and Table 1). We use these results to characterize the spatial and temporal scales of 65 WPEE events in section 4a. Then we separate these events into three groups to account for different underlying El Niño conditions in section 4b. Events before the El Niño onset, during the El Niño conditions, and the remaining events were designated as non-El Niño related.

Table 1. MJO-ids associated with a WPEE based on the underlying ENSO state, from 1998-2019.

ENSO conditions	Non-El Niño	Up to 9-months prior to El Niño	During El Niño
# events	25	17	23
MJO-ids	1,2,3,4,5,7,8,20,22,31, 46, 48,49,50,61, 62,63,66,67,70, 71,73,74,89,91	9, 10, 11, 12, 24, 25, 35, 36, 37, 38, 51, 75, 76, 77, 92,93, 94	13,14,15,16,17, 26,27,29,40,41,42,54, 55,56,57,59,80,81,84, 85,87, 97,98

Although most of MJO events that occurred before the onset of El Niño are associated with a WPEE (17 out of 25), a few events are associated with a warm pool retreat, likely associated with unfavorable large-scale atmospheric and oceanic conditions (Fig. 10c), and because these MJO events are weak as measured by rain and winds associated with the MJO, which will be further investigated quantitatively in Section 6.

The 33 remaining MJO events are associated with none WPEE or the warm pool retreat. A close examination of the lack of MJO activity in the western Pacific, when the

warm pool is far west located, during La Niña 1999-00 conditions is beyond the scope of this study. However, it raises interesting questions: is the lack of MJO events that lead to a strong and long-lasting La Niña event? Or the extreme La Niña conditions lead to reduced MJO activity in the western Pacific? Answering these questions is beyond the scope of this study and mechanism studies might be needed. However, Wu et al. (2019) argue that La Niña events' temporal evolution is strongly dependent on the intensity of the preceding El Niño event, indicating that unfavorable oceanic conditions for the MJO propagation in the western Pacific prevailed in 1999.

Although this paper focuses on MJO events that occurred before El Niño onset, some events occurred non-related to the El Niño condition but lead to a WPEE without developing the El Niño event that year. For example, MJO 1-2 and 61-63, earlier in 1999 and 2011, respectively, induced a WPEE for up to 2,000 km (Fig. 10a, Appendix Figure A1), which slowed down the equatorial negative warm pool anomalies, SST cooling, and trade winds, a few after the events (Fig. 10c-d). MJO Events from December 2016 – February 2017 (MJO 89-91) were associated with weaker warmer anomalies immediately after the events. We describe these events in Section 6.

a. MJO-induced WPEE

We characterize the MJO-induced WPEE using the equatorial band (5°S-5°N) from Day-0 to Day-Max for 65 events identified in section 2c-d. We composite the 65 events using the anomalous equatorial band grid points instead of the average because the WPEE is not monotonically, with both eastward and westward displacement as shown in Fig. 6 b-e. Figure 11a shows the frequency of the equatorial band grid points displacement over time after MJO events, as defined in Section 2c. Generally, an eastward displacement is more common (red

391 in Fig. 11a), especially during the first 15-20 days; but some westward displacement also
392 occurs (blue colors in Fig. 11a).

393 The joint histogram showed in Fig. 11 is computed using the equatorial band grid points
394 displacement as a function of days after the MJO events. The most frequent WPEE occurs
395 during the first 15-18 days with displacements up to 1,000 km (Fig. 10b). These spatial and
396 temporal scales give a WPEE speed range of about 0.6-0.8 m s^{-1}, close to the eastward
397 Yoshida jet speed (1m s^{-1}, Yoshida 1959; Ralph et al. 1996), but slower than ocean Kelvin
398 wave s (2 m s^{-1}). Assuming that an MJO-westerly event occurs at 150°E and the warm pool
399 eastern edge is located between 170°E-175°W, the time it takes for the oceanic Kelvin wave
400 to reach the warm pool edge is 12-22 days. On average, the WPEE duration and displacement
401 that occur after MJO events are within the range of an oceanic Kelvin wave propagation.
402 However, other processes at these short-timescales are also at work (e.g., non-linear
403 advection terms, strong zonal salinity gradient in driving surface currents jets, air-sea fluxes).

404 Less often but significant WPEE occurs beyond 25 days (Fig. 11a, b). To complete the
405 composite analysis, the number of MJO events that produced WPEE is shown in Fig. 11c.
406 The majority of events (60%, 40/65) during the first 15 days. Only 30% (20/65) sustained a
407 WPEE after 20 days (Fig. 11c) that occurred on a variety of ENSO conditions. Most events
408 (13/20) with sustained WPEE do not occurred during El Niño condition (Appendix Figure
409 A1e).

410 Based on the post-MJO WPEE observed in Fig.10, particularly consecutive events that
411 occurred before the El Niño onset, the next sub-section examines the MJO position on the
412 western Pacific in relation to the WPEE based on the three groups shown in Table. Events
413 before the El Niño onset, during the El Niño conditions, and non-El Niño related events that
414 includes neutral and La Niña conditions.

b. MJO-induced WPEE in relation to El Niño

We hypothesize that the local impacts of the MJO on the WPEE depends on its position in the western Pacific relative to the warm pool eastern edge on a first approximation. A broader MJO zonal fetch that reaches the vicinity of the warm pool edge induces a larger WPEE. Similarly, an off-equatorially MJO propagating feature, far away from the warm pool edge, might have a less direct impact on the WPEE. To test this idea, we compare the MJO propagation extent and the WPEE within each in Table 1.

The initial and ending longitude location provides the zonal MJO propagation extent, shown by the MJO track for each event within each group (Fig. 12 a-c). The composite the net WPEE as a function of latitude is obtained as the average of the warm pool anomaly at Day-Max minus the warm pool anomaly at Day-0 (Fig. 12 d-f). The WPEE confidence intervals at 95% of significance for each group (Fig. 12 d-f) indicate that the anomalous eastward displacement is a robust signal on each group. MJO events in the group before El Niño onset induce larger anomalous WPEE (up to 1,000 km), especially in the equatorial region but pronounced in the equatorial band and northern hemisphere. In contrast, the non-El Niño related group is associated with a relatively short displacement (800 km, Fig. 12d). The warm pool is already in an unusual eastern position in the El Niño group (not shown), and further eastward expansion of about 1,000 km is observed (Fig. 12f), mostly associated with the El Niño development (Kessler and Kleeman 2000, Eisenman et al. 2005).

The MJO impact on the warm pool is slightly pronounced on the northern tropical hemisphere (0-7°N versus 0-7°N) for the before El Niño onset group and during the El Niño group (Fig. 12e, f). One explanation comes from the large spatial variability of the warm pool eastern edge (Fig. 3) and the MJO proximity to it. MJO events from January-April are more likely to reach the warm pool eastern edge located at 170°E, 0-7°N (Fig. 3) and induce an

eastward expansion. In contrast, MJO events from June-August will have a less direct impact on the eastern edge unless MJO events propagate further east to the vicinity of the WP. MJO events over the equatorial region will have a less direct impact on the southern hemisphere (2-3°S-10°S); the warm pool is too far east located (Fig. 3) unless MJO events propagate south into the South Pacific Convergence Zone (SPCZ), which occurs during boreal winter (Fig. 14). The examination of the MJO impact too far off the equator is beyond the scope of this study.

Examining the number of MJO-induced WPEE by month (Fig. 15 a, b), we have confirmed that there are more MJO events in boreal winter than the rest year.

The MJO-induced WPEE for the groups non associated with El Niño development is a robust signal. The following analysis shows how much is the net SST change due to the post-MJO WPEE, particularly for the prior to El Niño onset group.

c. Composite of MJO-induced WPEE prior to El Niño

The MJO-induced WPEE of the before El Niño onset and non-El Niño related groups contributes with a net and significant (95% level) warming signal up to 0.5°C that extends from 1875°E-150°W and 10°S-10°N (Appendix Figure A2c). However, the most substantial warming located on the equator is associated with MJO events before El Niño onset group (Fig. 13c). Most importantly, a large portion of the MJO-induced warming before the onset of El Niño shown in Fig. 13c is located within the Niño 3.4 region (east of 170°W) with anomalies above 0.5°C. This result indicates that these MJO events directly contribute to the SST increase in Niño 3.4 and thus contributes to the onset of El Niño.

Given that tropical convection tends to be more active over the warmest SST, the initial MJO induced warming can promote further westerlies and drain the warm pool further eastward. The occurrence of multiple MJO events in the western Pacific associated is often

463 associated with a progressive warm pool eastward displacement, particularly during boreal
464 winter, and is discussed in the following section.

465 5. Seasonal variability of the MJO and WPEE

466 *a. Annual cycles of the MJO and MJO-induced WPEE*

467 The MJO events and induced WPEE have a pronounced seasonal cycle. MJO events in
468 the western Pacific are more frequently observed during boreal winter and early spring,
469 shifting towards the SPCZ (Fig. 14a). On the other hand, weak MJO activity occurs in
470 summer and fall with centers of convection shifting towards the northern hemisphere, when
471 the Asian monsoon is active. Likewise, the equatorial warm pool has a pronounced annual
472 cycle; it migrates from 170°E to 170°W from boreal Spring to Summer (dashed blue line in
473 Fig. 14b). However, the post-MJO equatorial warm pool displacement is located far beyond
474 the climatology position, especially from February to June during neutral ENSO conditions
475 (orange tick lines in Fig. 14b).

476 The MJO events with significant impact on the WPEE often occur during boreal spring;
477 these events can sustain anomalous displacements beyond 2,000 km (Fig. 15). These results
478 are consistent with previous studies (Moore and Kleeman 1999; Hendon et al. 2007) that
479 identified boreal spring as the time when the growth of ENSO SST anomalies is most
480 sensitive to MJO forcing. According to these arguments, if MJO activity is elevated during
481 spring, the WPEE leads to strong basin-wide warm SST anomalies in the Pacific (McPhaden
482 et al. 2006), leading to the development of El Niño the following boreal winter as was
483 demonstrated with robust lagged-correlations between MJO-filtered equatorial variables
484 (OLR and zonal surface windspeed) and Niño 3.4 SST index by Hendon et al. (2007).
485 However, Fig. 15 also shows that very significant anomalous displacement can occur during

boreal year-round for the non-El Niño related group, while MJO events before El Niño onset often happen in the first half of the year. Why these MJO evolve into an El Niño event can be explained by the background oceanic condition, but it is not explored in this study. However, we explore the MJO differences in terms of intensity of convection and westerlies and the WPEE for the non-El Niño group and before the El Niño onset group in section 6.

6. Intensity of the MJO and WPEE

To further quantify how the post-MJO WPEE is related to the strength of the MJO, we use the MJO intensity as a metric to compare individual and consecutive MJO events and associated WPEE in relation to onset of El Niño. The 33 MJO events during El Niño (highlighted in dark red in Fig. 10) are excluded to ensure that the WPEE is not a response to underlying El Niño conditions. We examine a total of 65 events, from which 42 are classified as post-MJO WPEE and 23 are associated with a warm pool westward displacement or non-displacement (Appendix Figure A1). Events that occurred before the onset of El Niño (25 events) are highlighted in red squares, and the rest are shown in gray circles. The MJO intensity in terms of Rain Volume varies from 0.3 to 16 x 10^8 m^3 with a mean of 5 x 10^8 m^3, and in terms of WWBs varies from 2 to 9 m s^{-1} with a mean of 5.7 m s^{-1} (Fig. 16 a-c).

Generally, the WPEE associated with individual events increases with the amount of rainfall and intensity of WWB (Fig 16a, b). Most MJO events (17 out of 25) that precede El Niño onset are characterized by large rain volume and strong WWBs, and they are associated with anomalous WPEE, beyond 500 km (Fig. 16 a, b). 8 out of 25 MJO events prior to El Niño event were related to the warm pool westward displacement despite being relatively intense events. These events happened during unfavorable conditions. For example, very intense trade winds (also called easterly winds events) can act against the WPEE and retreat

509 the initial eastward displacement as observed in June 2014 (e.g., MJO78, 79 in Fig., 10,
510 Appendix Figure A4). Strong trade winds in the central Pacific are also observed during the
511 following events: MJO-34, MJO-52,53, MJO-78,79.

512 The large spread between MJO intensity and WPEE suggest that the relationship is
513 complex and can be explained as follows: (i) each MJO event is different in duration and
514 structure (Fig. 1), and therefore the MJO intensity over the warm pool is expected to be
515 different (Fig. 2); (ii) the impact of each MJO on the WPEE depends on its relative position
516 to the warm pool eastern edge; and (iii) the net WPEE response to an MJO event depends on
517 the oceanic and atmospheric state, as pointed out by previous studies (e.g., Bergman et al.
518 2001; Fedorov et al., 2015, and Puy et al., 2019).

519 Consecutive MJO events can affect the ocean state on long timescales, as
520 demonstrated by previous studies (e.g., Kessler and Kleeman 2000; Bergman et al. 2001). To
521 examine the net impact of consecutive MJO events on the WPEE, we quantitatively measure
522 consecutive MJO events' strength. Some consecutive MJO events are associated with a
523 progressive eastward warm pool expansion. For example, MJO 1-2 events observed in 1999
524 (Fig. 10, Appendix Figure A3), and MJO 75-77 events that occurred during neutral
525 conditions before the strong El Niño 2015 event (Fig. 10, Appendix Figure A4). We found
526 six cases that occurred before El Niño onset (9-12, 23-25, 35-39, 51-53, 75-77, and 92-94),
527 three during El Niño conditions (16-17, 54-59, 75-76), and five cases during cold or neutral
528 conditions (1-2, 5-8,61-63, 67-68, 89-91). We do not include events during El Niño
529 conditions, and red squares to are used to highlight consecutive events that happen prior to
530 the El Niño onset (six groups) and circles to highlight the remaining consecutive MJO events
531 (4 groups) in Fig. 16d. The Rain Volume representative of a group of consecutive MJO
532 events is the accumulated Rain Volume of individual events, and the WWB corresponds to

533 the maximum within the group. Grouped MJOs Rain Volume and WWB are shown in Fig.
534 16d colored by the total WPEE and with marker sizes proportional to the number of events,
535 the smallest circles are individual events. The total WPEE is quantified as the accumulation
536 of individual displacements.

537 As expected, larger WPEE is associated with consecutive MJO LPTs with strong
538 WWBs and large accumulated Rain Volume, especially before the onset of El Niño. Each El
539 Niño event from 1998-2019 was preceded by 3 to 5 MJO events within 9 months before their
540 onset. These grouped MJO events are associated with significant anomalous WPEE varying
541 from 1,500 to 4,000 km. These results support the premise that the MJO group effort has a
542 more significant impact on the WPEE.

543 The large WPEE associated with consecutive MJO events are the result of the long-
544 term effect of MJO forcing on the upper ocean and is commonly observed as large-scale SST
545 anomalies in the equatorial Pacific Ocean that often produce large-scale wind anomalies (Fig.
546 9 a-c and Fig. 13c), that under favorable can allow further growth of coupled atmosphere-
547 ocean processes allowing the warm pool to shift further east during the onset of El Niño (Fig
548 9 d-e).

549 Consecutive MJO events not related to El Niño (circles in Fig. 16d) are also strong in
550 convection and westerlies; however, they happen under non favorable atmospheric (strong
551 trade winds) and oceanic conditions (Fig. 10c) and induced a relatively short WPEE. The
552 maximum total anomalous WPEE (2,600 km) from the non-El Niño related group observed
553 in Fig. 16d (red circle) correspond to the consecutive MJO 5-8 events that lead to the
554 transition from neutral condition in January-April 2001 and initial warm anomalies in May
555 2001 (Fig. 10d).

556 The consecutive MJO-rainfall impact on the warm pool long timescales of variability
557 is unknown to our knowledge. However, the large-scale and sustained MJO-rainfall during its
558 propagation over the warm pool as observed in Fig. 16d (15-30 10^8 m^3) affect the freshwater
559 fluxes. The MJO-rainfall changes the upper ocean salinity that could play an active role.
560 Freshwater fluxes affect the zonal density contrast across the warm pool eastern edge, which
561 further impact the horizontal pressure gradient and zonal currents (Lengaigne et al., 2003,
562 Roemmich et al., 1994). Freshwater fluxes enhance favorable conditions for barrier layer
563 formation and strengthening (Vialard et al. 1998). Further investigation is needed to confirm
564 the rainfall-impact on the warm pool associated with consecutive MJO events but before El
565 Niño onset.

566 The following questions remain to be answered. Where is the maximum MJO impact
567 on the warm pool in terms of rain and westerlies? Are the MJO prior to El Niño significantly
568 stronger than the non-El Niño related group? To address these questions, we use composites
569 of the accumulated volume rain and the averaged WWB inside the MJO LPTs feature from
570 5°S-5°N throughout the MJO lifetime, every 0.25° in longitude (Fig 17). To contrast the
571 group of non-El Niño related from the group prior to El Niño onset, we computed confidence
572 intervals at 95% level, shown in gray and red shading, respectively, in Fig 17.

573 Composites of rain volume and WWB along the MJO LPTs propagation show the
574 location of the MJO-rainfall and WWBs impact in the warm pool. It increases gradually from
575 130°E to 150°E, in both groups. However, events before the El Niño onset group are
576 significantly stronger at 95% than the non-El Niño related group, especially east to 150°E.
577 These results indicate that MJO events prior to El Niño events propagate further east than the
578 remaining events, the net local MJO impact, 150°E - 170°E, affect SST anomalies to east as
579 observed in Fig. 13c.

7. Summary and conclusions

This study investigates the relationship of the MJO and the WPEE. For the first time, we are able to quantify the time and spatial scales of the MJO-induced WPEE in connection to the onset of El Niño using satellite-observed precipitation, surface wind, and SST data, we have quantified, for the first time, the time and spatial scales of the MJO-induced WPEE in the equatorial Pacific region (10°S – 10°N).

The 20-year MJO events database obtained from the LPT algorithm allowed to quantify the MJO-induced WPEE for individual events, the MJO intensity of convection and westerlies and the location of impact. The MJO-induced WPEE was quantified using the warm pool easternmost longitude displacement and its anomaly relative to a 30-years climatology. Both methods gave essentially the same results, and we used the WPEE anomaly (Section 2. c, d).

The majority of MJO events (65%) induced a WPEE of 1000 km during 15 days after the MJO event passage over the western Pacific. Up to 20% of MJO events induced a continuous and long-lasting (> 20 days) anomalous WPEE beyond 1000 km (Fig. 11), beyond 3,000 km for the absolute WPEE. Quantifying the timing and scale of the MJO-induced WPEE can be useful to predict subsequent precipitation and WWBs given that tropical convection is restricted to the warm SST region, which can increase the eastward migration of the warm pool and can generate equatorial waves resulting in remote SST impacts.

There is a distinct characteristic that distinguishes MJO events that precede El Niño onset. They are notably stronger and propagate further east, characterized by large Rain Volume and strong WWBs (Fig. 16, 17), and can induce a significant anomalous WPEE (> 1000 km) or absolute WPEE (> 2000 km) that is sufficiently robust and maintained beyond

604 the annual cycle (Fig. 12-15). The MJO rainfall and WWBs are noticeable higher on the
605 equator (5°S - 5°N) from 150°E - 170°E, west of the Niño 3.4 region (Fig. 17). More
606 importantly, these events contribute with a net and large-scale warm SST anomaly above
607 0.5°C to Niño 3.4, thus contributing to El Niño onset (Fig. 13).

608 Consecutive MJO events induce much larger WPEE and are observed before each El
609 Niño event over the 20 years studied (Fig. 16d). The intensity of rain volume and WWBs of
610 the grouped consecutive MJO events is directly related to the WPEE distance. The
611 consecutive MJO impact on the ocean has long-term atmospheric and oceanic implications.
612 They are often reflected as a change in the trade winds intensity and the subsurface
613 temperature across the equatorial Pacific basin, as observed before El Niño onset 2002-03
614 and 2018-19 (Figs. 7-9). These results raise interesting questions. For instance, how many
615 MJO events are needed to weaken the strong trade winds, and how they depend on the ocean
616 conditions. How does the atmosphere-ocean couple change in response to consecutive MJO
617 events (e.g., zonal pressure gradient across the warm pool in response to freshwater fluxes)?

618 There is a distinct seasonal variability in the MJO events and the induced WPEE.
619 During Boreal winter and early spring (Fig. 14), the MJO's track density reaches the
620 dateline's vicinity (Fig. 12). Significant anomalous WPEE (> 1000 km) occurs during the
621 transition from Boreal Spring to Summer (Fig. 15c, d), which coincides with the warm pool's
622 seasonal migration (Fig. 3). These results emphasize the role of MJO forcing on the western
623 Pacific during Boreal spring when the zonal SST gradient is weak, and the atmosphere-ocean
624 coupled system is unstable to SST changes (Latif et al. 1994).

625 Several key conclusions can be drawn from the results presented in this study:

626 • about 65% of the MJO events induced a WPEE up to 3000 km along the
627 equator, which can last beyond 15 days;

- the MJO events that precede the onset of El Niño are generally stronger and produce significant WPEE far beyond its annual cycle (~1000 km);
- consecutive MJO events can produce much larger WPEE prior to El Niño, which are observed in all El Niño events from 1998-2019; but also observed during non-El Niño years; and
- more frequent and *larger* MJO-induced WPEE occur in March-May than other seasons.

These results can help understand the MJO-ENSO interaction and improve the prediction of the onset of El Niño.

It should also note that the results described in this study are based on just over 20 years of satellite observations. Although these observations showed enhanced MJO activity followed by a WPEE leading to each El Niño event's onset, they do not consider the broad-spectrum of ENSO. It has been suggested that the ENSO regime shifted around 1999-00 to more frequent central Pacific El Niño events (McPhaden 2012, Hu et al., 2017). Whether the MJO frequency in the western Pacific has changed and how it is connected to ENSO is beyond this study's scope. However, based on the dominant mechanisms that explain the MJO-induced WPEE with potential impact on the El Niño onset (e.g., Kessler et al. 1995, Shinoda and Hendon 2001, Zhang and Gottschalck 2002), and based on the robust lagged MJO-ENSO correlation for 1979-2005 showed by Hendon et al. (2007), the connection between the MJO-induced WPEE and El Niño onset for 1979-2005 might still hold.

The improvements of coupled global simulations with far better resolution and more developed physical parameterizations have improved the simulation of crucial characteristics of ENSO and MJO. However, there is still room for improvement regarding their forecast skill, especially for forecasts that start in Boreal spring (Barnston et al. 2012, Zhao et al.

2016, Cai et al. 2019). With the advancement of further modeling development and the tropical Pacific observing system (TPOS) effort, studies explaining the mechanism(s) responsible for the atmosphere-ocean interaction are needed. Understanding how atmospheric processes (e.g., MJO) affect mixed-layer temperature and provide feedback to the atmosphere for a range of spatial and temporal timescales is critical to understanding ENSO variability.

This study should help evaluate atmosphere-ocean coupled simulations on the Pacific on a range of timescales. Reproducing the right location and intensity of the MJO rain and westerly winds at occurs at relatively short timescales (Fig.17) could improve the SST response to MJO forcing (Fig. 13), which could improve the representation of the large-scale gradient that drives the circulation in the equatorial Pacific at the onset of El Niño. On long timescales, a good representation of the MJO forcing over the warm pool might reduce the climatological warm pool edge bias observed in the CMIP5 models (Brown et al., 2014). The current modeling projections of the MJO and ENSO in response to global warming are still uncertain. However, the "wet get wetter" thermodynamic and dynamic response to this warming predicts that the large-scale rainfall over the warmest SSTs will increase (Held and Soden, 2006). How the precipitation and freshwater affect salinity and upper-ocean stratification on long-timescales? What is the ocean dynamics response to the ocean stratification and how it affects the development of ENSO or MJO? Improving the representation of the multiscale processes in Earth-system models will be critical in global weather and climate predictions. These questions motivate a follow-up study, which aims to improve our understanding of the physical mechanism(s) through which the MJO influences the eastward extension of the warm pool leading to the onset of El Niño 2018.

Acknowledgments.

We thank Brandon Kerns and Ajda Savarin for their assistance on the MJO LPT analysis, and Chidong Zhang for helpful discussions on the MJO and ENSO interaction. This research is supported by the NOAA CVP grants NA15OAR4320063 and NA18OAR4310401. The first author is partially supported by the National Fund for Scientific, Technological Development and Technological Innovation (FONDECYT), the funding branch of the National Council for Science, Technology and Technological Innovation (CONCYTEC) Peru (N° 094-2016-FONDECYT).

Data Availability Statement.

The data used in this paper were obtained from the Remote Sensing Systems (CCMP V2.0; www.remss.com), the NASA/Goddard Space Flight Center and archived at the NASA GES DISC online (TMPA data; https://disc.gsfc. nasa.gov/datasets/TRMM_3B42_ Daily_7/summary), the NOAA/OAR/ESRL PSL (High Resolution SST; https://psl.noaa.gov/) and the Climate Prediction Center (https://www.cpc.ncep.noaa.gov/data/indices/sstoi.indices). The MJO-LPT system database created by Kerns and Chen 2020 and used in this study is available online (http://orca.atmos.washington.edu/data/lpt).

694

695 REFERENCES

696 Anderson, S. P., R. A. Weller, and R. B. Lukas, 1996: Surface Buoyancy Forcing and the
697 Mixed Layer of the Western Pacific Warm Pool: Observations and 1D Model Results. *J.*
698 *Climate*, **9**, 3056–3085, https://doi.org/10.1175/1520-
699 0442(1996)009<3056:SBFATM>2.0.CO;2

700 Atlas, R., J. Ardizzone, and R. N. Hoffman, 2008: Application of satellite surface wind
701 data to ocean wind analysis. *Remote Sensing System Engineering*, **7087**, 118 – 124,
702 https://doi.org/10.1117/12.795371

703 Barnston, A. G., M. K. Tippett, M. L. L'Heureux, S. Li, and D. G. DeWitt, 2012: Skill of
704 real-time seasonal ENSO model predictions during 2002–2011: Is our capability increasing?
705 *Bull. Amer. Meteor. Soc*., **93**, 631– 651, https://doi.org/10.1175/BAMS-D-11-00111.1.

706 Battisti, D. S., D. J. Vimont, and B. P. Kirtman, 2019: 100 Years of progress in
707 understanding the dynamics of coupled atmosphere/ocean variability 100 Years of progress
708 in understanding the dynamics of coupled atmosphere/ocean variability. *Meteor.*
709 *Monographs*, **59**, 8.1– 8.57, https://doi.org/10.1175/AMSMONOGRAPHS-D-18-0025.1

710 Bergman, J. W., H. H. Hendon, and K. M. Weickmann, 2001: Intraseasonal Air–Sea
711 Interactions at the Onset of El Niño. *J. Climate*, **14**, 1702–1719, https://doi.org/10.1175/1520-
712 0442(2001)014<1702:IASIAT>2.0.CO;2

713 Brown, J.N., C. Langlais, and C. Maes, 2014: Zonal structure and variability of the
714 Western Pacific dynamic warm pool edge in CMIP5. *Clim Dyn* **42**, 3061–3076.
715 https://doi.org/10.1007/s00382-013-1931-5

716

Bosc, C., T. Delcroix, and C. Maes, 2009: Barrier layer variability in the western Pacific warm pool from 2000 to 2007. *J. Geophys. Res.,* **114,** C06023, https://doi.org/10.1029/2008JC005187.

Boulanger, J.P. and C. Menkes, 1999: Long equatorial wave reflection in the Pacific Ocean from TOPEX/POSEIDON data during the 1992–1998 period. *Clim Dynam* **15**, 205–225.

Cai, W., and Coauthors, 2019: Pantropical climate interactions. *Science*, **363**, 6430, https://doi.org/10.1126/science.aav4236.

Cane, M. A., 1986: EL Nino. *Annual Review of Earth and Planetary Sciences*, 14 (1), 43–70, https://doi.org/10.1146/annurev.ea.14.050186.000355.

Chen, S. S., R. A. Houze, Jr. and B. E. Mapes, 1996: Multiscale variability of deep convection in relation to large-scale circulation in TOGA COARE. *J. Atmos. Sci.*, **53**, 1380-1409.

Chen, S. S., and R. A. Houze, Jr., 1997a: Diurnal variation and lifecycle of deep convective systems over the tropical Pacific warm pool. *Quat. J. Roy. Meteor. Soc*., **123**, 357-388.

Chen, S. S., and R. A. Houze, Jr., 1997b: Interannual variability of deep convection over the tropical warm pool. *J. Geophys. Res.*, **102**, 25,783-25,795.

Chen, S. S., W. Zhao, J. E. Tenerelli, R. H. Evans, V. Halliwell, 2001: Impact of the Pathfinder sea surface temperature on atmospheric forcing in the Japan/East Sea, *Geophys. Res. Lett.*, **28**, No. 24, 4539-4542, https://doi.org/10.1029/2001GL013511.

740 Chiodi, A. M., D.e. Harrison, and G.A. Vecchi, 2014: Subseasonal Atmospheric
741 Variability and El Niño Waveguide Warming: Observed Effects of the Madden–Julian
742 Oscillation and Westerly Wind Events*. *J Clim* **27**, 3619–3642.

743 Clarke, A. J., J. Wang, and S. V. Gorder, 2000: A Simple Warm-Pool Displacement
744 ENSO Model. *J. Phys. Oceanogr.*, **30 (7)**, 1679–1691, https://doi.org/10.1175/1520-
745 0485(2000)030<1679:ASWPDE>2.0.CO;2.

746 CPC, 2017. Cold and Warm Episodes by Season.
747 https://origin.cpc.ncep.noaa.gov/products/analysis_monitoring/ensostuff/ONI_v5.php

748 Delcroix, T., J.-P. Boulanger, F. Masia, and C. Menkes, 1994: Geosat-derived sea level
749 and surface current anomalies in the equatorial pacific during the 1986–1989 el Niño and la
750 Niña. *J. Geophys. Res: Oceans*, **99 (C12)**, 25093–25107, https://doi.org/10.1029/94JC02138.

751 Drushka, K., H. Bellenger, E. Guilyardi, M. Lengaigne, J. Vialard, and G. Madec, 2015:
752 Processes driving intraseasonal displacements of the eastern edge of the warm pool: the
753 contribution of westerly wind events. *Climate Dynamics*, **44 (3-4)**, 735–755,
754 https://doi.org/10.1007/s00382-014-2297-z.

755 Eisenman, I., L. Yu, and E. Tziperman, 2005: Westerly Wind Bursts: ENSO's Tail Rather
756 than the Dog? *J. Climate*, **18 (24),** 5224–5238, https://doi.org/10.1175/JCLI3588.1.

757 Fasullo, J., and P. J. Webster, 2000: Atmospheric and surface variations during westerly
758 wind bursts in the tropical Pacific, *Q. J. R. Meteorol. Soc.,* **126**, 899–924.

759 Fedorov, A. V., and S. G. Philander, 2001: A Stability Analysis of Tropical Ocean–
760 Atmosphere Interactions: Bridging Measurements and Theory for El Niño. *J. Climate*, **14**
761 **(14)**, 3086–3101, https://doi.org/10.1175/1520-0442(2001)014<3086:ASAOTO>2.0.CO;2.

762 Fedorov, A. V., S. Hu, , M. Lengaigne and E. Guilyardi, 2015: The impact of westerly
763 wind bursts and ocean initial state on the development, and diversity of El Niño events. *Clim*
764 *Dynam* **44**, 1381–1401.

765 Harrison, D. E., and B. S. Giese, 1991: Episodes of surface westerly winds as observed
766 from islands in the western tropical Pacific. *J. Geophys. Res.*, **96 (S01)**, 3221,
767 https://doi.org/10.1029/90JC01775.

768 Harrison, D. E., and P. S. Schopf, 1984: Kelvin-Wave-Induced Anomalous Advection
769 and the Onset of Surface Warming in El Niño Events. *Mon. Wea. Rev.*, **112**, 923–933,
770 https://doi.org/10.1175/1520-0493(1984)112<0923:kwiaaa>2.0.co;2.

771 Held, I. M., and B. J. Soden, 2006: Robust responses of the hydrological cycle to global
772 warming, J. Clim., **19**, 5686–5698.

773 Hendon, H. H., M. C. Wheeler, and C. Zhang, 2007: Seasonal Dependence of the MJO–
774 ENSO Relationship. *J. Climate*, **20 (3)**, 531–543, https://doi.org/10.1175/jcli4003.1.

775 Hu, Z.-Z., A. Kumar, B. Huang, J. Zhu, and H.-L. Ren, 2017a: Interdecadal variations of
776 ENSO around 1999/2000. *J. Meteor. Res.*, **31**, 73–81, https://doi.org/10.1007/s13351-017-
777 6074-x.

778 Huffman, G. J., and Coauthors, 2007: The TRMM Multisatellite Precipitation Analysis
779 (TMPA): Quasi-Global, Multiyear, Combined-Sensor Precipitation Estimates at Fine Scales.
780 *Journal of Hydrometeorology*, **8 (1)**, 38–55, https://doi.org/10.1175/jhm560.1.

781 Jin, F.-F., 1997: An equatorial ocean recharge paradigm for ENSO. Part I: Conceptual
782 model. *J. Atmos. Sci.*, **54**, 811–829, https://doi.org/10.1175/1520-
783 0469(1997)054<0811:AEORPF>2.0.CO;2.

784 Kerns, B. W., and S. S. Chen, 2016: Large-scale precipitation tracking and the MJO over
785 the Maritime Continent and Indo-Pacific warm pool. *J. Geophys. Res.: Atmospheres*, **121**
786 **(15)**, 8755–8776, https://doi.org/10.1002/2015jd024661.

787 Kerns, B. W., and S. S. Chen, 2020: A 20-Year Climatology of Madden-Julian
788 Oscillation Convection: Large-Scale Precipitation Tracking From TRMM-GPM Rainfall. *J.*
789 *Geophys. Res.: Atmospheres*, **125 (7)**, https://doi.org/10.1029/2019jd032142.

790 Kessler, W. S., 2002: Is ENSO a cycle or a series of events? *Geophys. Res. Lett.*, ***29(23)***,
791 2125, https://doi.org/10.1029/2002gl015924.

792 Kessler, W. S., and R. Kleeman, 2000: Rectification of the Madden–Julian Oscillation
793 into the ENSO Cycle. *J. Climate*, **13 (20)**, 3560–3575, https://doi.org/10.1175/1520-
794 0442(2000)013<3560:ROTMJO>2.0.CO;2.

795 Kessler, W. S., M. J. McPhaden, and K. M. Weickmann, 1995: Forcing of intraseasonal
796 Kelvin waves in the equatorial Pacific. *J. Geophys. Res.*, **100 (C6)**, 10613,
797 https://doi.org/10.1029/95JC00382.

798 Latif, M., T. P. Barnett, M. A. Cane, M. Flügel, N. E. Graham, H. v. Storch, J. S. Xu, and
799 S. E. Zebiak, 1994: A review of ENSO prediction studies. *Climate Dynamics*, **9 (4-5)**, 167–
800 179, https://doi.org/10.1007/bf00208250.

801 Lau, K.-M., and P. H. Chan, 1988: Intraseasonal and interannual variations of tropical
802 convection: A possible link between the 40–50 day oscillation and ENSO? *J. Atmos. Sci.*, **45**
803 **(3)**, 506–521, https://doi.org/10.1175/1520-0469(1988)045<0506:IAIVOT>2.0.CO;2.

804 Lengaigne, M., J. Boulanger, C. Menkes, S. Masson, G. Madec, and P. Delecluse, 2002:
805 Ocean response to the March 1997 Westerly Wind Event. *J. Geophys.* Res.: Oceans, **107**
806 **(C12)**, 8015, https://doi.org/10.1029/2001JC000841.

Lengaigne, M., J.-P. Boulanger, C. Menkes, G. Madec, P. Delecluse, E. Guilyardi, and J. Slingo, 2003: The March 1997 Westerly Wind Event and the Onset of the 1997/98 El Niño: Understanding the Role of the Atmospheric Response. *J. Climate*, **16 (20),** 3330–3343, https://doi.org/10.1175/1520-0442(2003)016<3330:tmwwea>2.0.co;2.

Lindzen, R. S., and S. Nigam, 1987: On the Role of Sea Surface Temperature Gradients in Forcing Low-Level Winds and Convergence in the Tropics. *J. Atmos. Sci*, **44 (17)**, 2418–2436, https://doi.org/10.1175/1520-0469(1987)044<2418:OTROSS>2.0.CO;2.

Lukas, R., and E. Lindstrom, 1991: The mixed layer of the western equatorial Pacific Ocean. *J. Geophys. Res.: Oceans*, **96 (S01)**, 3343–3357, https://doi.org/10.1029/90jc01951.

Madden, R. A., and P. R. Julian, 1971: Detection of a 40–50 Day Oscillation in the Zonal Wind in the Tropical Pacific. *J. Atmos. Sci*, **28 (5)**, 702–708, https://doi.org/10.1175/1520-0469(1971)028<0702:doadoi>2.0.co;2.

Madden, R. A., and P. R. Julian, 1972: Description of Global-Scale Circulation Cells in the Tropics with a 40–50 Day Period. *J. Atmos. Sci*, **29 (6)**, 1109–1123, https://doi.org/10.1175/1520-0469(1972)029<1109:dogscc>2.0.co;2.

Madden, R. A., and P. R. Julian, 1994: Observations of the 40–50-Day Tropical Oscillation—A Review. *Monthly Weather Review*, **122 (5)**, 814–837, https://doi.org/10.1175/1520-0493(1994)122<0814:OOTDTO>2.0.CO;2.

Maes, C., Picaut, J., and S. Belamari, 2005. Importance of the salinity Barrier Layer for the Buildup of El Niño. *J. Climate*, **18(1),** 104 –118. https://doi.org/10.1175/jcli-3214.1.

Maes, C., K. Ando, T. Delcroix, W. S. Kessler, M. J. McPhaden, and D. Roemmich, 2006: Observed correlation of surface salinity, temperature and barrier layer at the eastern

edge of the western Pacific warm pool. *Geophys. Res. Lett.,* **33 (6),** https://doi.org/10.1029/2005gl024772.

Maes, C., M. J. McPhaden, and D. Behringer, 2002: Signatures of salinity variability in tropical Pacific Ocean dynamic height anomalies. *J. Geophys. Res.: Oceans*, **107 (C12)**, 8012, https://doi.org/10.1029/2000JC000737.

Marshall, A. G., O. Alves, and H. H. Hendon, 2009: A Coupled GCM Analysis of MJO Activity at the Onset of El Niño. *J. Atmos. Sci*, **66 (4),** 966–983, https://doi.org/10.1175/2008jas2855.1.

McPhaden, M. J., and J. Picaut, 1990: El Niño-Southern Oscillation Displacements of the Western Equatorial Pacific Warm Pool. *Science*, **250 (4986)**, 1385–1388, https://doi.org/10.1126/science.250.4986.1385.

McPhaden, M. J., and X. Yu, 1999: Equatorial waves and the 1997–98 El Niño. *Geophys. Res. Lett.*, **26 (19),** 2961–2964, https://doi.org/10.1029/1999gl004901.

McPhaden, M. J., 2004: Evolution of the 2002/03 El Niño*. *Bull. Amer. Meteor. Soc.,* **85 (5),** 677–695, https://doi.org/10.1175/bams-85-5-677.25.

McPhaden, M. J., S. E. Zebiak, and M. H. Glantz, 2006: ENSO as an Integrating Concept in Earth Science. *Science*, **314 (5806)**, 1740–1745, https://doi.org/10.1126/science.1132588.

McPhaden, M., Zhang, X., Hendon, H., Wheeler, M, 2006. Large scale dynamics and MJO forcing of ENSO variability. *Geophys. Res. Lett*. **33(16)**, https://doi.org/10.1029/2006gl026786.

McPhaden, M. J., 2012: A 21st century shift in the relationship between ENSO SST and warm water volume anomalies. *Geophys. Res. Lett.*, **39**, L09706, https://doi.org/10.1029/2012GL051826.

852 Mechem, D. B., S. S. Chen, and R. A. Houze, Jr., 2005: Momentum transport processes
853 in the stratiform regions of mesoscale convective systems over the western Pacific warm
854 pool, *Quat. J. Roy. Meteor. Soc*., **132A**, 709-736, https://doi.org/10.1256/qj.04.141.

855 Moore, A. M., and R. Kleeman, 1999: Stochastic Forcing of ENSO by the Intraseasonal
856 Oscillation. *J. Climate*, **12 (5),** 1199–1220, https://doi.org/10.1175/1520-
857 0442(1999)012<1199:SFOEBT>2.0.CO;2.

858 Neelin, J. D., D. S. Battisti, A. C. Hirst, F.-F. Jin, Y. Wakata, T. Yamagata, and S. E.
859 Zebiak, 1998: ENSO theory. *J. Geophys. Res.: Oceans*, **103 (C7)**, 14261–14290,
860 https://doi.org/10.1029/97jc03424.

861 Philander, S. G. H., T. Yamagata, and R. C. Pacanowski, 1984: Unstable air-sea
862 interactions in the tropics. *J. Atmos. Sci*, **41 (4)**, 604–613, https://doi.org/10.1175/1520-
863 0469(1984)041<0604:UASIIT>2.0.CO;2.

864 Picaut, J., and T. Delcroix, 1995: Equatorial wave sequence associated with warm pool
865 displacements during the 1986–1989 El Niño-La Niña. *J. Geophys. Res.: Oceans*, **100 (C9),**
866 18393–18408, https://doi.org/10.1029/95JC01358.

867 Picaut, J., M. Ioualalen, T. Delcroix, F. Masia, R. Murtugudde, and J. Vialard, 2001: The
868 oceanic zone of convergence on the eastern edge of the Pacific warm pool: A synthesis of
869 results and implications for El Niño-Southern Oscillation and biogeochemical phenomena. *J.*
870 *Geophys. Res.: Oceans*, **106 (C2)**, 2363–2386, https://doi.org/10.1029/2000JC900141.

871 Picaut, J., F. Masia, and Y. d. Penhoat, 1997: An Advective-Reflective Conceptual Model
872 for the Oscillatory Nature of the ENSO. *Science*, **277 (5326)**, 663–666,
873 https://doi.org/10.1126/science.277.5326.663.

874

875 Puy, M., J. Vialard, M. Lengaigne, and E. Guilyardi, 2016: Modulation of equatorial
876 Pacific westerly/easterly wind events by the Madden–Julian oscillation and convectively-
877 coupled Rossby waves. *Clim Dynam* **46**, 2155--2178.

878 Puy, M., J. Vialard, M. Lengaigne, E. Guilyardi, A. Voldoire, M. Gurvan, 2019:
879 Modulation of equatorial Pacific sea surface temperature response to westerly wind events by
880 the oceanic background state. *Clim Dynam* **52**, 7267–729.

881 Ralph, E. A., Bi, K., Niiler, P. P. & Penhoat, Y. du., 1997: A Lagrangian Description of
882 the Western Equatorial Pacific Response to the Wind Burst of December 1992: Heat
883 Advection in the Warm Pool. *J Climate*, **10**, 1706–1721, https://doi.org/10.1175/1520-
884 0442(1997)010<1706:ALDOTW>2.0.CO;2.

885 Reynolds, R. W., N. A. Rayner, T. M. Smith, D. C. Stokes, and W. Wang, 2002: An
886 Improved in situ and Satellite SST Analysis for Climate. *J. Climate*, **15(13),** 1609–1625,
887 https://doi.org/10.1175/1520-0442(2002)015<1609:AIISAS>2.0.CO;2.

888 Reynolds, R. W., T. M. Smith, C. Liu, D. B. Chelton, K. S. Casey, and M. G. Schlax,
889 2007: Daily High-Resolution-Blended Analyses for Sea Surface Temperature. *J. Climate*, **20**
890 **(22)**, 5473–5496, https://doi.org/10.1175/2007JCLI1824.1.

891 Roemmich, D., M. Morris, W. R. Young, and J. R. Donguy, 1994: Fresh Equatorial
892 Jets. J Phys Oceanogr **24**, 540–558.

893 Rui, H., and B. Wang, 1990: Development Characteristics and Dynamic Structure of
894 Tropical Intraseasonal Convection Anomalies. *J. Atmos. Sci*, **47 (3),** 357–379,
895 https://doi.org/10.1175/1520-0469(1990)047<0357:DCADSO>2.0.CO;2.

Seiki A. and Y.N. Takayabu, 2007: Westerly wind bursts and their relationship with intraseasonal variations and ENSO. Part II: energetics over the Western and Central Pacific. Mon Wea Rev 135:3346–3361. doi:10.1175/MWR3477.1

Suzuki, T. & Takeuchi, K., 2000: Response of Equatorial Pacific Mean Temperature Field to Intraseasonal Wind Forcing. *J Oceanogr*, **56**, 485–494, https://doi.org/10.1023/A:1011140708962.

Vecchi, G. A., and D. E. Harrison, 2000: Tropical Pacific Sea Surface Temperature Anomalies, El Niño, and Equatorial Westerly Wind Events*. *J. Climate*, **13 (11)**, 1814–1830, https://doi.org/10.1175/1520-0442(2000)013<1814:TPSSTA>2.0.CO;2.

Vialard, J., and P. Delecluse, 1998: An OGCM Study for the TOGA Decade. Part II: Barrier- Layer Formation and Variability. *J. Phys. Oceanogr.*, **28 (6)**, 1089–1106, https://doi.org/10.1175/1520-0485(1998)028<1089:AOSFTT>2.0.CO;2.

Vialard, J., P. Delecluse, and C. Menkes, 2002: A modeling study of salinity variability and its effects in the tropical Pacific Ocean during the 1993-1999 period. *J. Geophys. Res.: Oceans,* **107 (C12)**, https://doi.org/10.1029/2000JC000758.

Wang, B., and T. Li, 1994: Convective Interaction with Boundary-Layer Dynamics in the Development of a Tropical Intraseasonal System. *J. Atmos. Sci*, **51 (11)**, 1386–1400, https://doi.org/10.1175/1520-0469(1994)051<1386:CIWBLD>2.0.CO;2.

Wang, S.-Y., M. L'Heureux, and H.-H. Chia, 2012: ENSO prediction one year in advance using western North Pacific sea surface temperatures. *Geophys. Res. Lett.*, **39 (5)**, L05702, https://doi.org/10.1029/2012GL050909.

Wyrtki, K., 1975: El Niño—The Dynamic Response of the Equatorial Pacific Ocean to Atmospheric Forcing. *J. Phys. Oceanogr.*, **5(4)**, 572–584, https://doi.org/10.1175/1520-0485(1975)005<0572:ENTDRO>2.0.CO;2.

Wyrtki, K., 1985: Water displacements in the Pacific and the genesis of El Nino cycles. *J. Geophys. Res.*, 90 **(C4)**, 7129, https://doi.org/10.1029/JC090iC04p07129.

Wu, X., Okumura, Y., DiNezio, P. (2019). What Controls the Duration of El Niño and La Niña Events? What Controls the Duration of El Niño and La Niña Events? J. Climate, **32(18)**, 5941-5965, https://doi.org/10.1175/JCLI-D-18-0681.1.

Yano, J.-I., R. Blender, C. Zhang, and K. Fraedrich, 2004: 1/f noise and pulse-like events in the tropical atmospheric surface variabilities. *Quarterly Journal of the Royal Meteorological Society*, **130 (600)**, 1697–1721, https://doi.org/10.1256/qj.03.42.

Yoshida, K., 1959: A Theory of the Cromwell Current (the Equatorial Undercurrent) and of the Equatorial Upwelling. *Journal of the Oceanographical Society of Japan*, **15 (4)**, 159–170, https://doi.org/10.5928/kaiyou1942.15.159.

Yu, L., R. A. Weller, and W. T. Liu, 2003: Case analysis of a role of ENSO in regulating the generation of westerly wind bursts in the Western Equatorial Pacific. *J. Geophys. Res.: Oceans*, **108**, 3128, https://doi.org/10.1029/2002JC001498.

Zhang, C., 2005: Madden-Julian Oscillation. *Reviews of Geophysics*, **43 (2)**, https://doi.org/10.1029/2004RG000158.

Zhang, C., 2013: Madden–Julian Oscillation: Bridging Weather and Climate. *Bull. Amer. Meteor. Soc.,* **94 (12)**, 1849–1870, https://doi.org/10.1175/BAMS-D-12-00026.1.

Zhang, C., Hendon, H., Kessler, W., & Rosati, A. (2001). A Workshop on the MJO and ENSO. *Bull. Amer. Meteor. Soc., **82(5)***, 971-976.

940 Zhang, C., and J. Gottschalck, 2002: SST Anomalies of ENSO and the Madden–Julian
941 Oscillation in the Equatorial Pacific. *J. Climate*, **15 (17)**, 2429–2445,
942 https://doi.org/10.1175/1520-0442(2002)015<2429:SAOEAT>2.0.CO;2.

943 Zhao, M., H. H. Hendon, O. Alves, G. Liu, and G. Wang, 2016: Weakened eastern
944 Pacific El Niño predictability in the early twenty-first century. *J. Climate*, **29**, 6805–6822,
945 https://doi.org/10.1175/JCLI-D-15-0876.1.

946

947

948

949

950

951 FIGURES

952

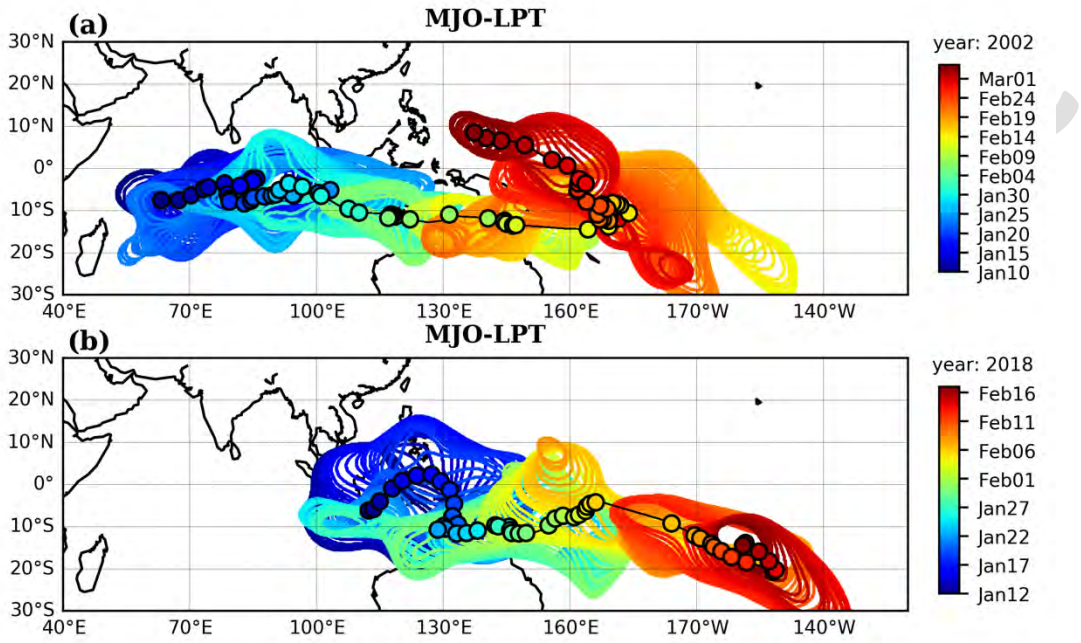

953

954 **Fig. 1** The MJO large-scale precipitation tracking (LPT) systems shown in color contours
955 evolving in time at 6-hourly interval for two MJO events: (a) January-March 2002 and
956 (b) January-February 2018 corresponding to MJO-11 and MJO-93 in Fig. 10. The
957 centroids of the MJO LPT are shown as black circles. The LPT uses 12 mm day^{-1}
958 threshold as described in Kerns and Chen (2020).

959

960

961

962

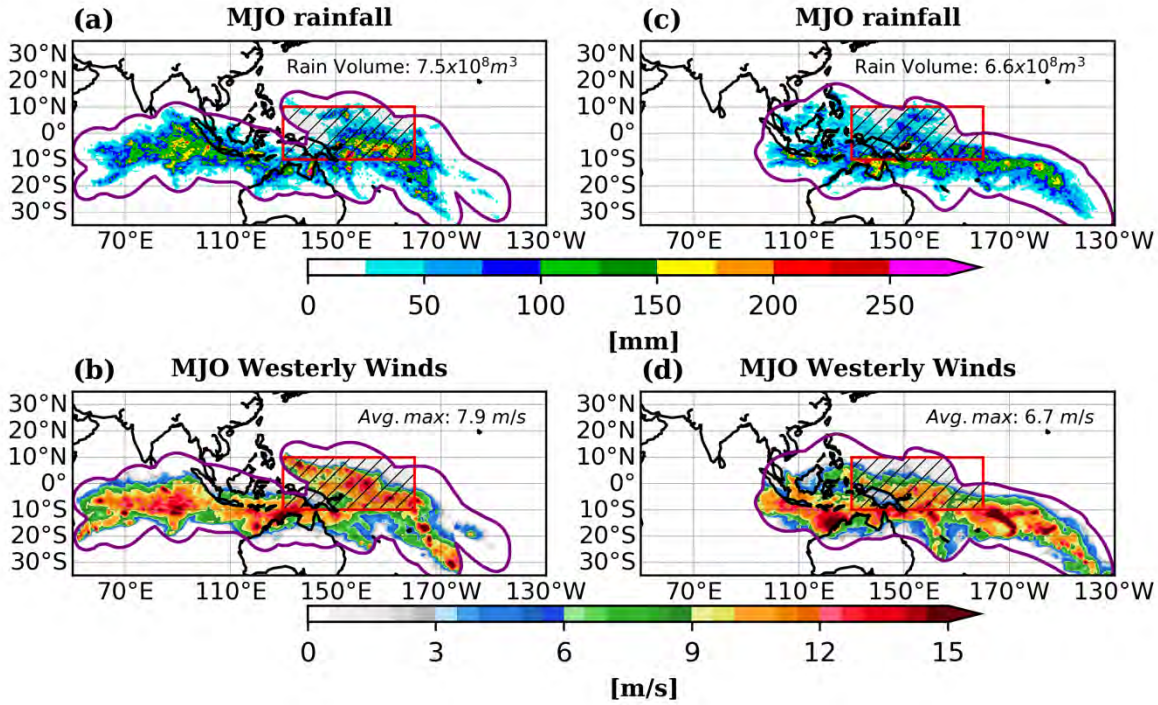

Fig. 2 The MJO envelope (purple contour) indicates the area encompassed by the MJO-LPT feature for the two MJO events as shown in Fig. 1, with (a, c) the cumulative rainfall in mm and (b,d) averaged westerly windspeed in m s^{-1} during the lifetime of MJO LPT systems. The red box marks the region of MJO impact on the warm pool (130°E-180 to 10°S-10°N). The total cumulative rain volume (m^3) and areal averaged windspeed (m s^{-1}) representing the westerly winds burst (WWB) within the red box are given at the top-right, respectively.

977

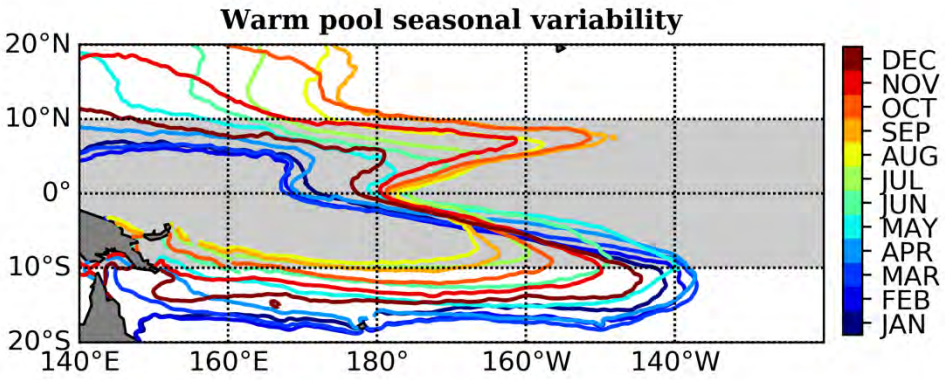

978

979 **Fig. 3** Monthly climatology of the warm pool (28.5°C) from Jan-Dec (color) computed using

980 the OISST-V2 data.

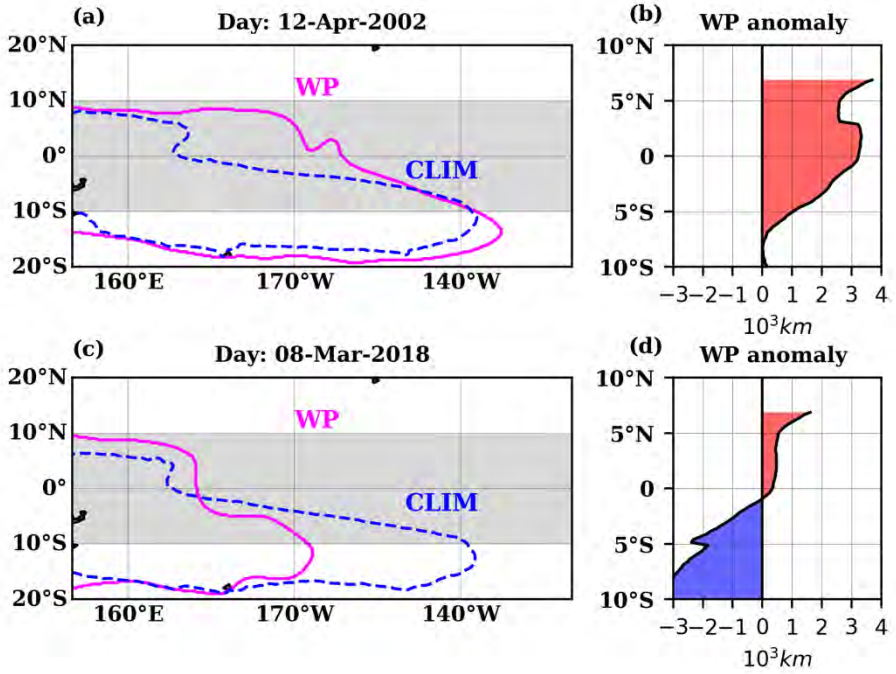

981

982 **Fig. 4** (a, c) The maximum eastward warm pool (28.5°C) positions on April 12, 2002 and

983 May 5, 2018, immediately after the two MJO events shown in Fig. 1 (magenta) and

984 corresponding daily climatology (blue dashed lines) , (b, d) anomalous WP positions

985 computed as a difference of the warm pool eastern-most longitude relative to its

986 climatology from 10°S to 10°N.

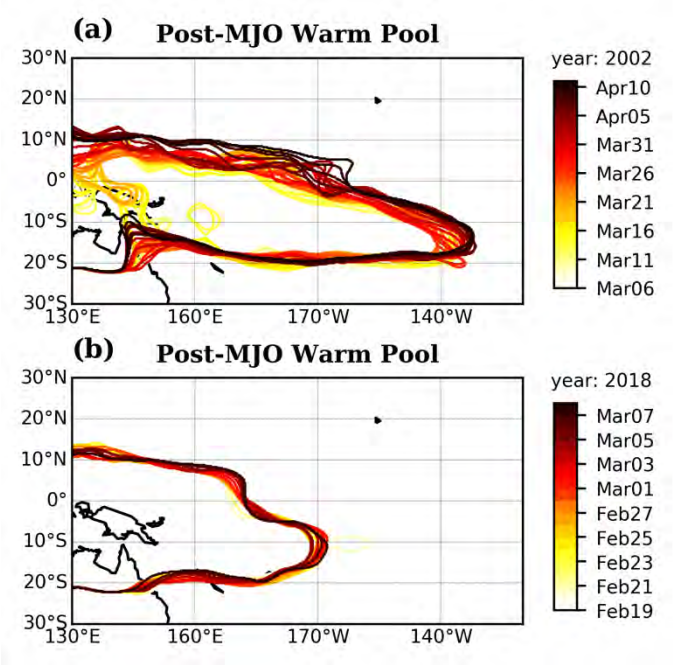

Fig. 5 The evolution of warm pool (28.5°C contour) after the two MJO events as shown in Fig. 1: (a) Mar-Apr 2002 and (b) Feb-Apr 2018 with dates in color.

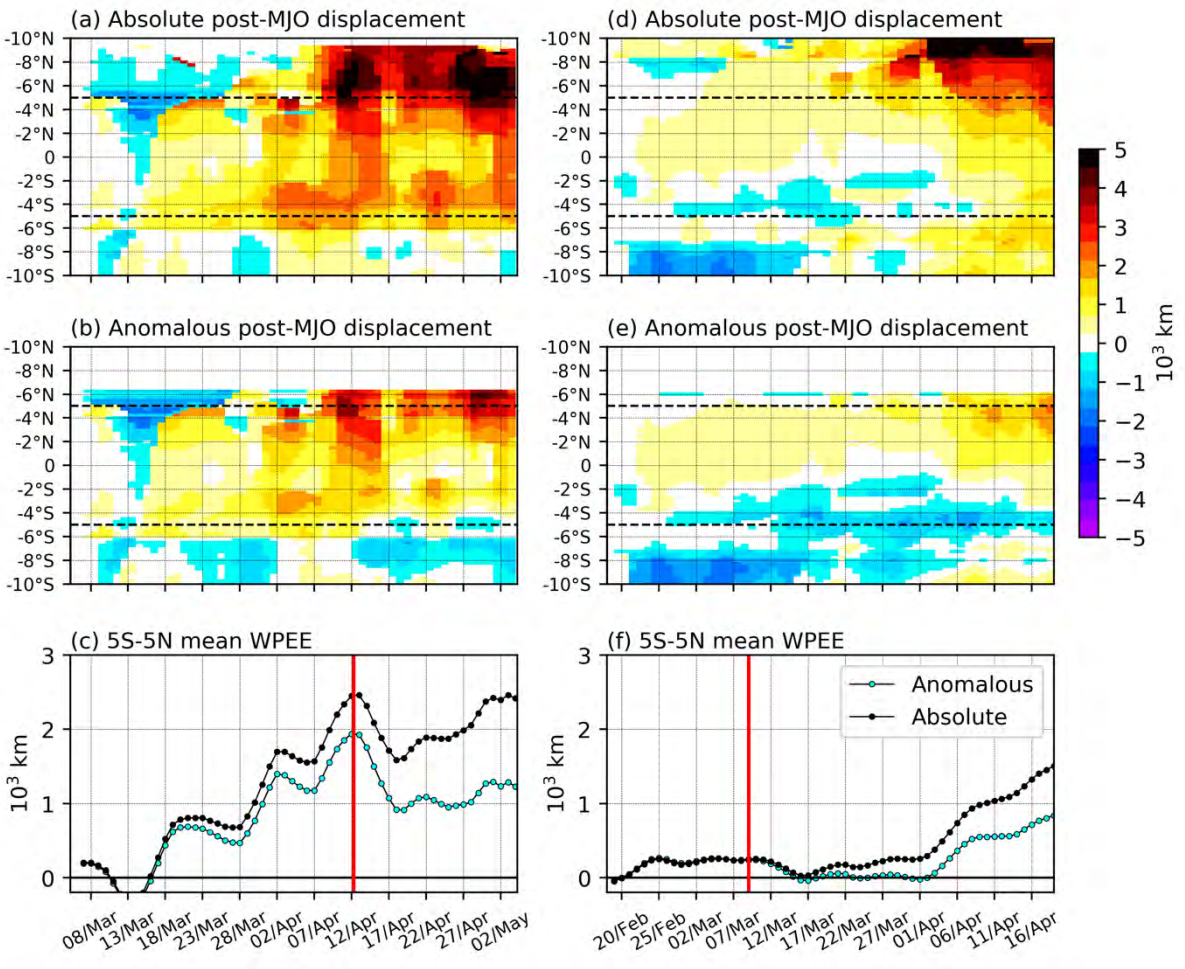

Fig. 6 (a, d) The post-MJO absolute warm pool displacement (10^3 km, color) over time relative to positions on March 5, 2002 and February 18, 2018, respectively, from 10°S–10°N. (b, e) Anomalous warm pool displacement in10^3 km relative to daily climatology. The black dashed line corresponds to the equatorial band (5°S-5°N) . (c, f) Averaged warm pool absolute (black) and anomalous (cyan) displacement from 5°S-5°N, where vertical red lines indicate the day of maximum anomalous eastward displacement (Day-max) immediately after the MJO events shown in Fig. 1.

1012

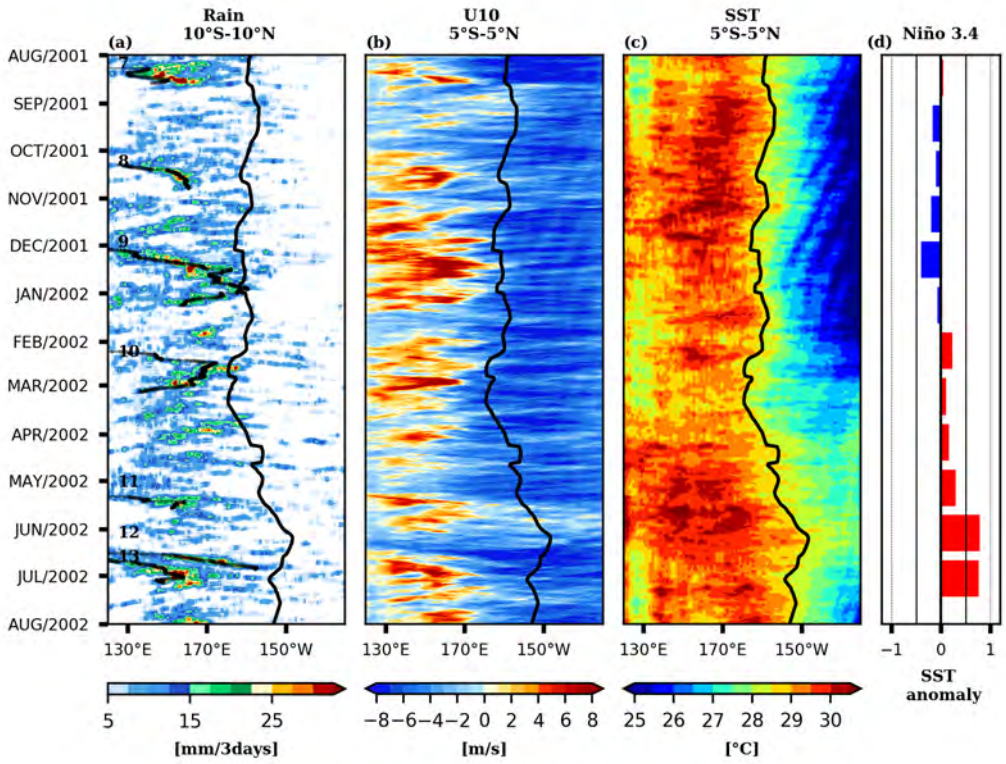

1013

1014 **Fig. 7** Time-longitude sections of (a) 3-day accumulated rainfall averaged from 10°S-10°N

1015 with the MJO LPT centroids for the events 7-13 (black dots) from August 2001-August

1016 2002, (b) 6-hourly absolute zonal surface windspeed averaged from 5°S-5°N, (c) daily

1017 SST average from 5°S-5°N, and (d) Niño 3.4 monthly anomalies. The position of

1018 equatorial warm pool is shown in black contours in (a)-(c).

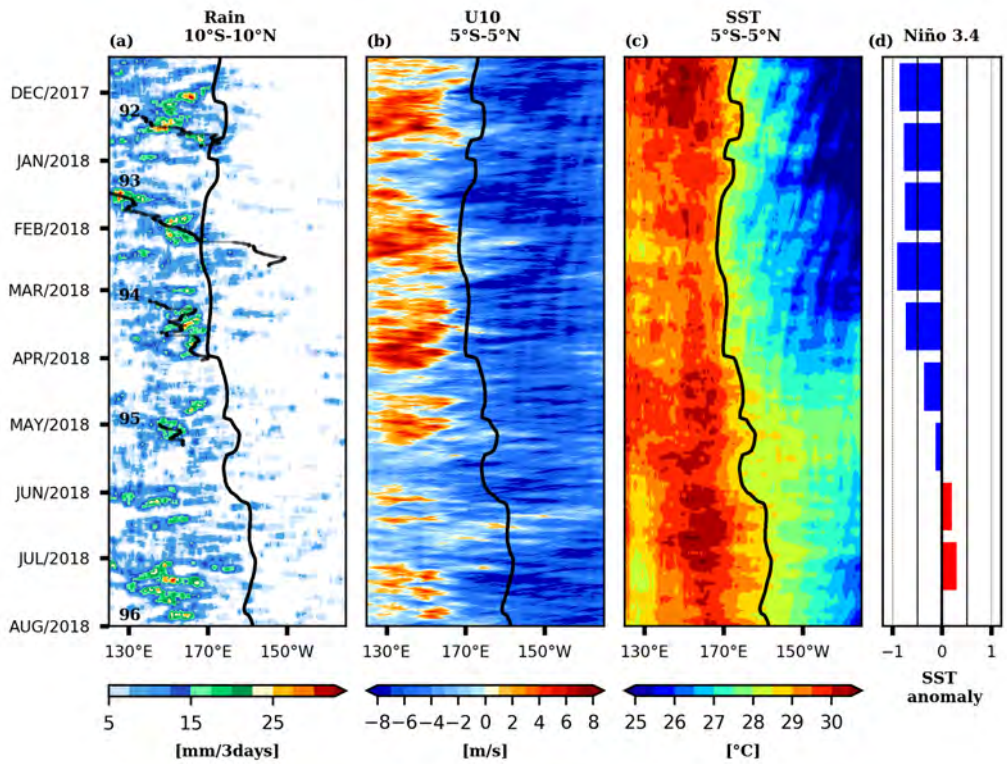

Fig. 8 Same as in Fig. 7 but from November 2017-August 2018.

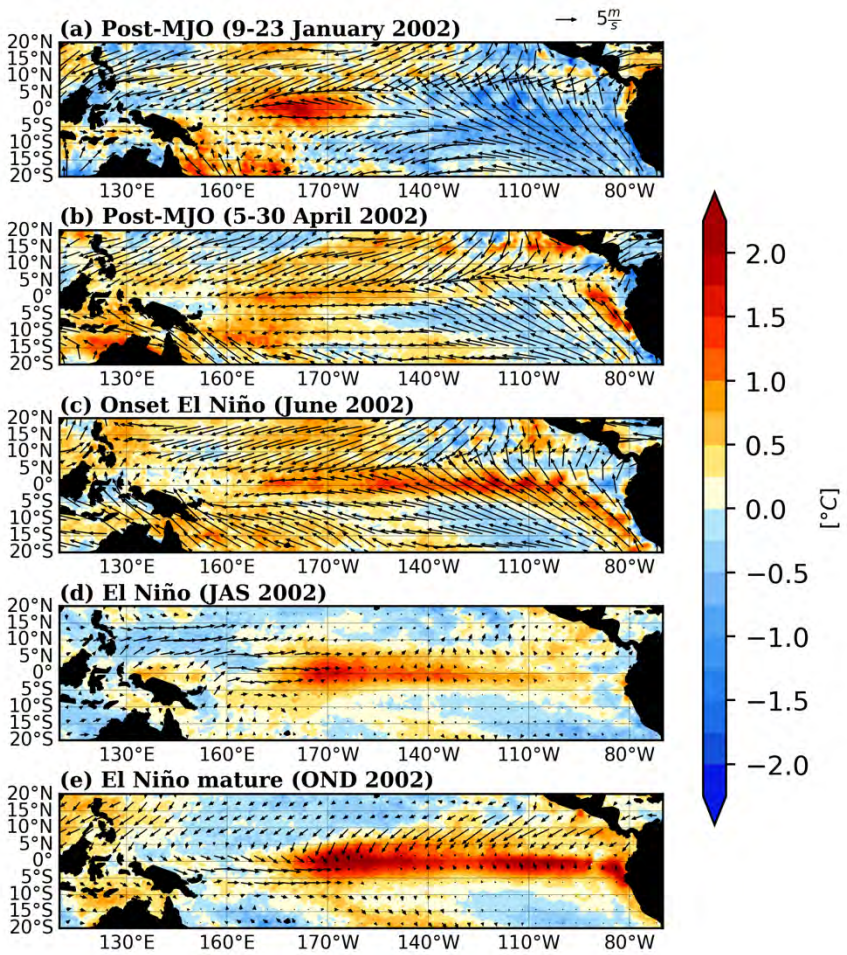

Fig. 9 Surface wind anomalies (vectors) and SST anomaly (colors, in °C) for two post-MJO periods from (a) 9-23 January 2002 associated with MJO-10 and (b) 5-30 April 2002 associated with MJO-11, (c) onset of the El Niño in June 2002**, (d)** maturing stages in June-August, and (e) September-November 2002.

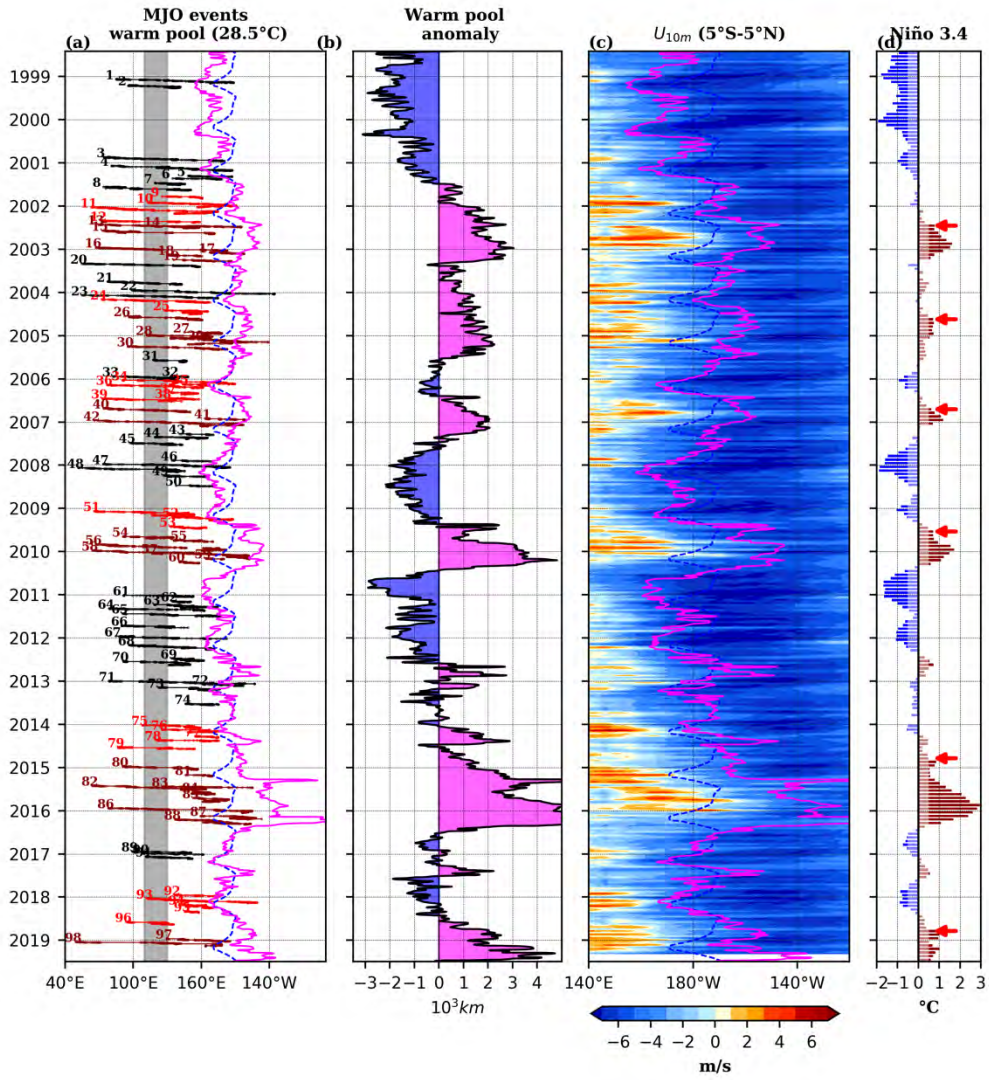

1041

1042 **Fig. 10** (a) The eastern edge of equatorial warm pool (28.5°C, magenta) and its climatological
1043 position (blue dashed) from 1998-2019. MJO events are shown in red when they occur
1044 within 9-months prior to the onset of El Niño , in darkred during El Niño and in the rest
1045 in (black). (b) The eastern edge equatorial warm pool anomaly (10^3km), blue and
1046 fuchsia are negative and positive anomalies, respectively. (c) Equatorial absolute
1047 surface zonal winds from CCMP. (d) Niño 3.4 SST anomaly (3-monthly averages,
1048 horizontal bars) highlighted in red (blue) for anomalies > 0.5°C (< -0.5°C). The onset
1049 of each El Niño events is indicated by red arrows. Gray background in panel (a) show
1050 longitudes 110°E-130°E. -

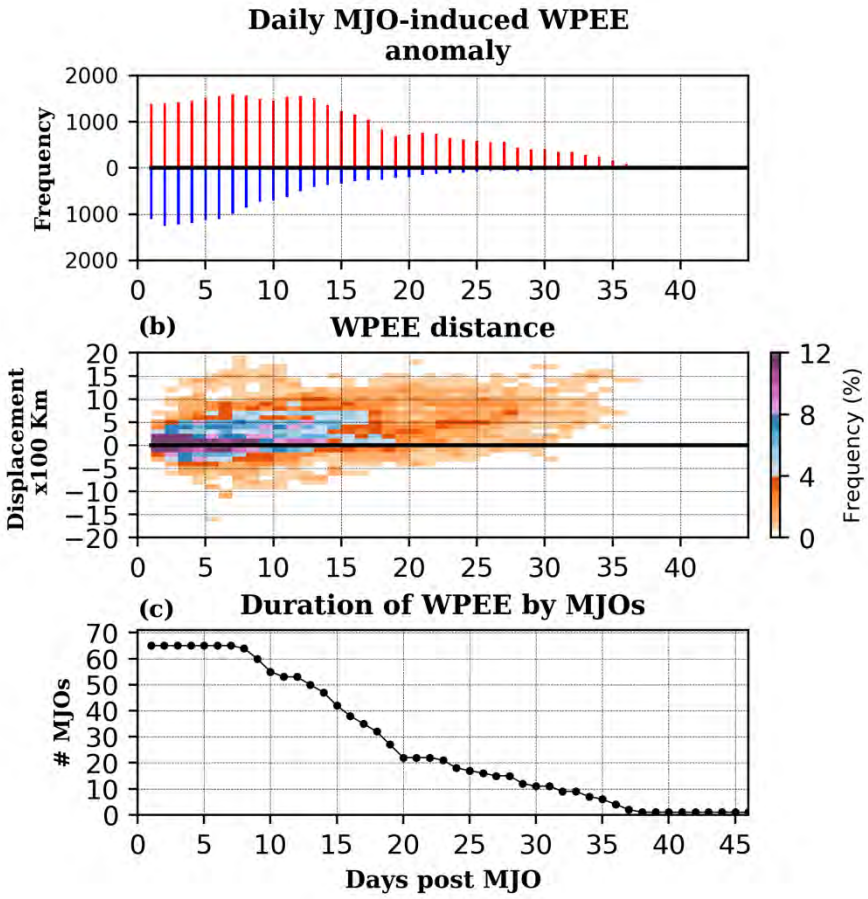

Fig. 11 Characteristic of the MJO-induced WPEE as a function of days post-MJO precipitation: (a) frequency of warm pool displacement (number of the equatorial band grids per day), eastward in red and westward in blue, (b) **joint** histogram of the warm pool eastern edge displacement (in 10^2 km) as a function of days post-MJO, and (c) number of the MJO that produced WPEE varying with time after the MJO.

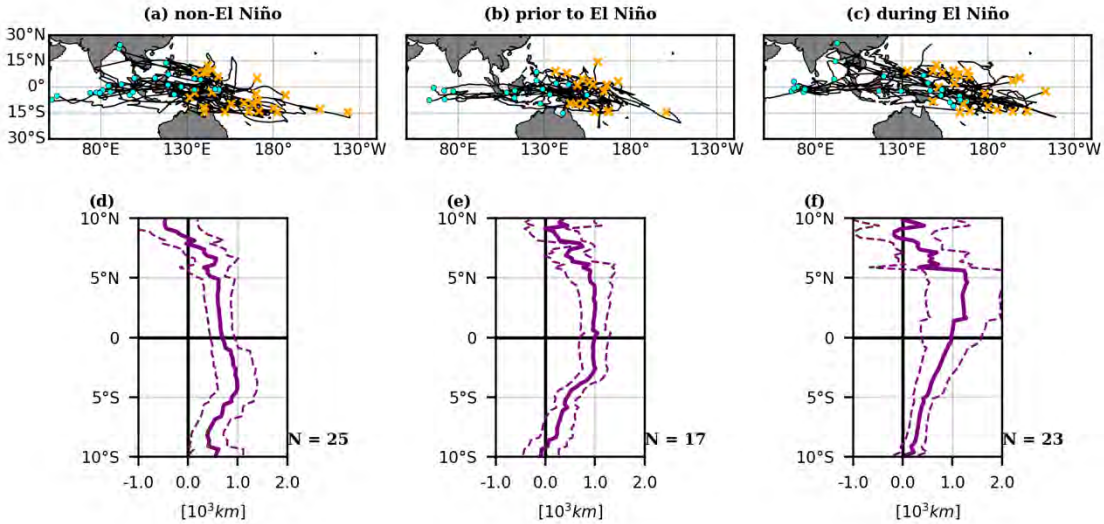

Fig 12. Centroid tracks of the MJO events for (a) non-El Nino related (25 events), (b) prior to El Nino (17 events), and (c) during El Nino (23 events). Cyan dots and orange crosses mark the start and end of the tracks. (d)-(f) The WPEE composite as a function of latitude, every 0.25°, computed as the difference of the warm pool anomaly (see section 2c or Fig. 4b, d) between Day-max and Day-0. Dashed lines show the confidence intervals ($\alpha = 0.05$).

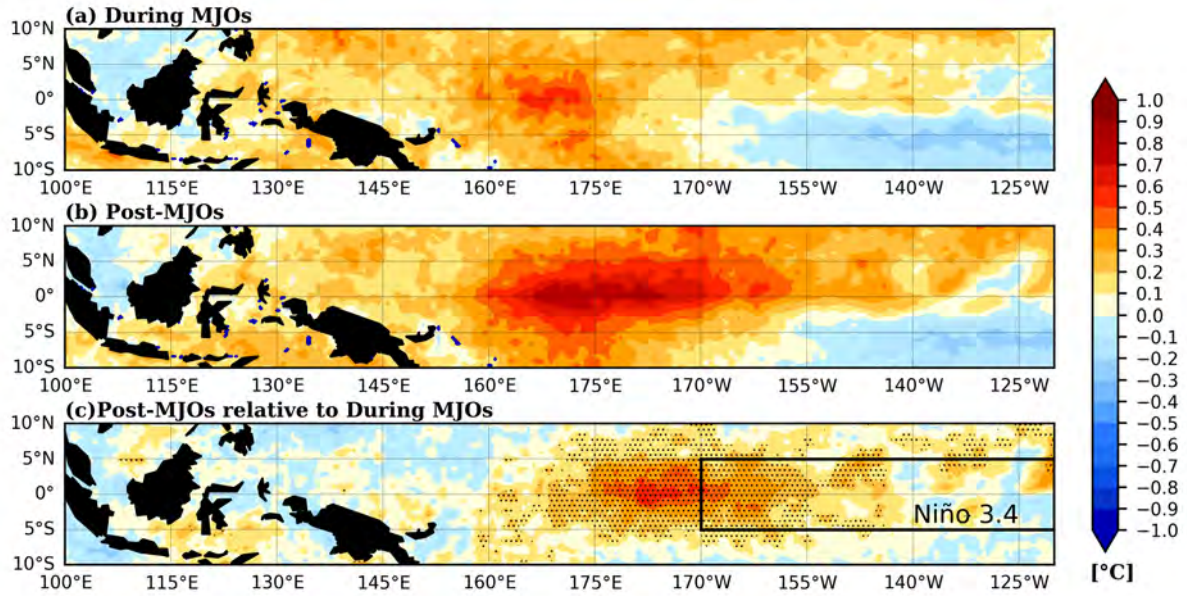

Fig. 13 Composite of SST anomaly for the MJO events prior to the onset of El Nino (a) during the MJO LPTs lifetime, (b) post-MJO period from Day-1 to Day-max, and (c) the difference between the post-MJO and the MJO SST anomaly. Black box indicates the Niño 3.4 region and hatched dots mark locations with significantly warmer at 95% confidence level.

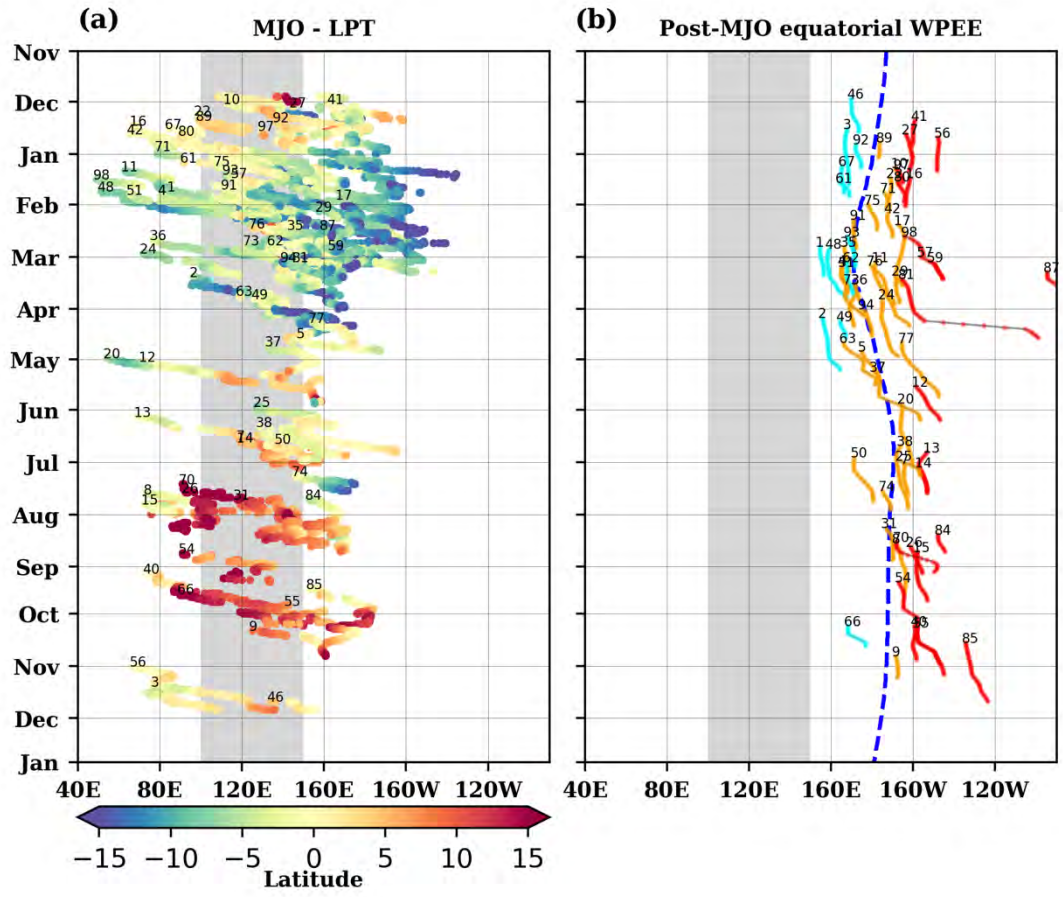

Fig. 14 (a) Annual cycle of the MJO LPTs for the 63 MJO from 1998-2019 that produced a post-MJO WPEE varying with longitude and latitude (color). Numbers are the MJO IDs. (b) The corresponding post-MJO equatorial WPEE. The dashed blue line marks the climatology of the eastern edge of the equatorial warm pool.

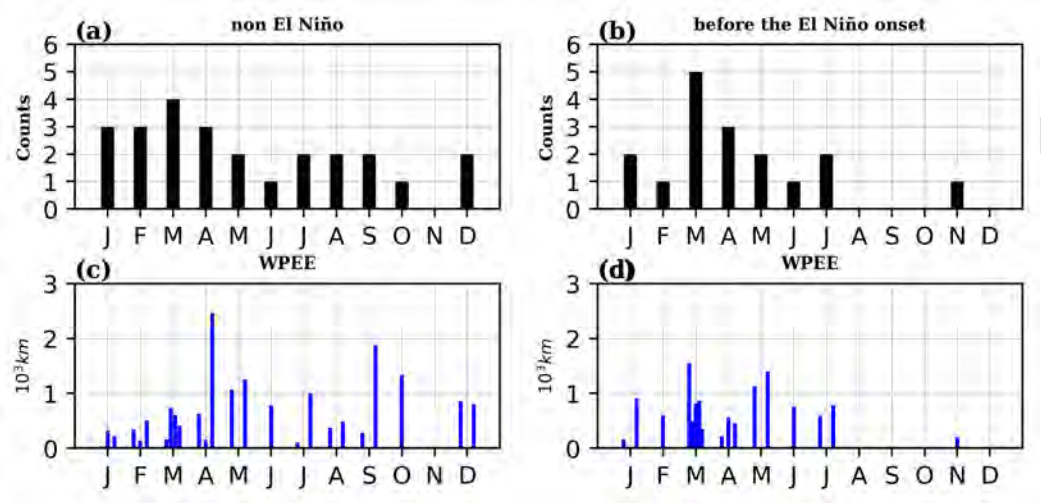

Fig. 15 Monthly variability of the MJO events: (a) non-El Niño related and (b) before the El Niño onset from 1998-2019. (c, d) The Max-WPEE (blue) associated with each MJO event shown in (a) and (b). DJF (December to February), MAM (March to May), JJA (June to August), SON (September to November).

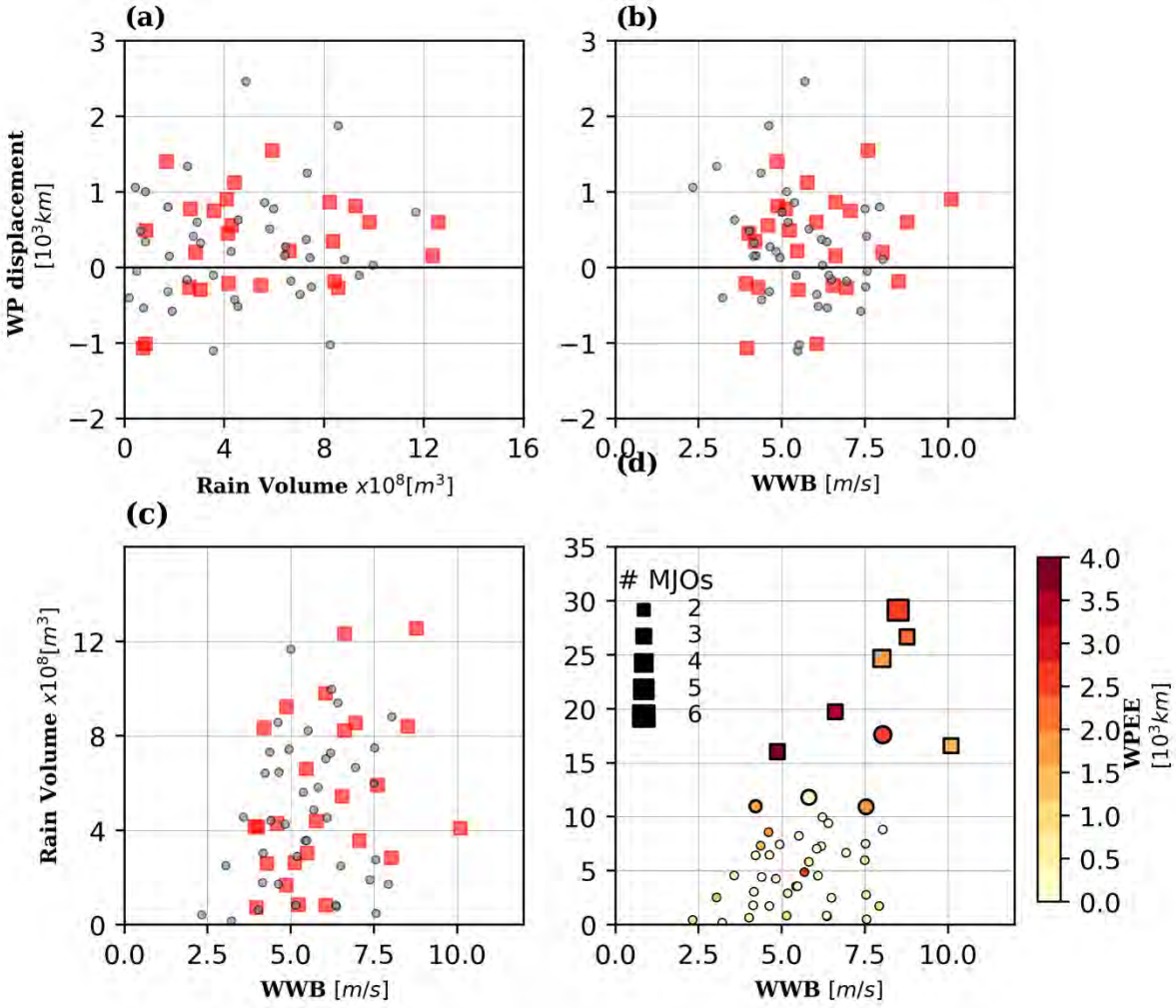

Fig. 16 Post-MJO warm pool displacement as a function of (a) total rain volume (m^3) of the MJO LPTs (b) WWB (averaged windspeed, m s^{-1}). The MJO events occurred prior to the El Nino onset are shown in red squares, and non-El Niño related in gray circles. (c) Total rain volume in relation to WWB for individual MJO LPTs with WPEE. (d) The MJO events prior to each El Nino onset are grouped together and their collective WPEE (km) are shown in color. There are 6 groups of consecutive MJO events prior to the

onset of each El Niño. The number of the MJO events in each group are proportional to the size of the squares. MJO events occurred during El Niño are excluded in all panels.

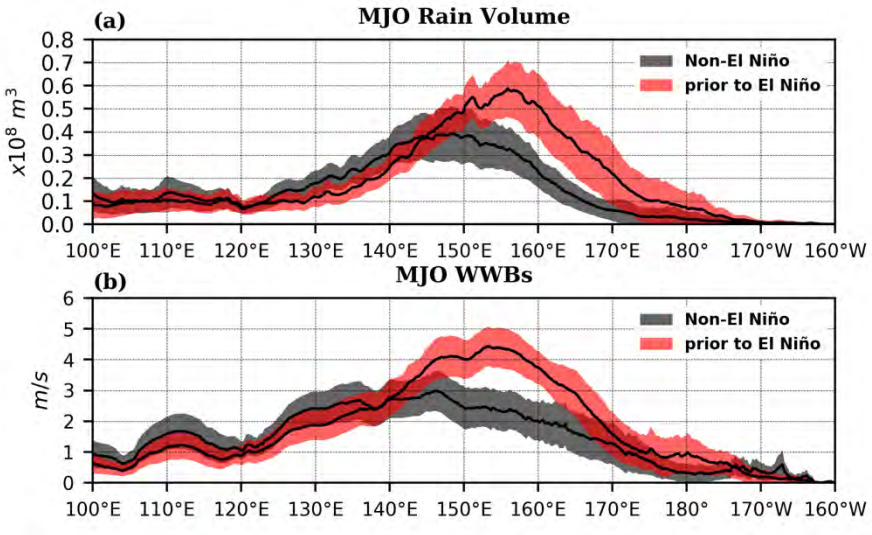

Fig. 17 (a) The total rain volume (m^3) of the MJO LPTs and (b) averaged WWB windspeed within the MJO LPTs from 5°S-5°N as a function of longitude. 95% confidence interval is shown for MJO events non-El Niño related (gray) and prior to El Niño onset (red).